Distribution Agreement

In presenting this thesis as a partial fulfillment of the requirements for a degree from Emory University, I hereby grant to Emory University and its agents the non-exclusive license to archive, make accessible, and display my thesis in whole or in part in all forms of media, now or hereafter now, including display on the World Wide Web. I understand that I may select some access restrictions as part of the online submission of this thesis. I retain all ownership rights to the copyright of the thesis. I also retain the right to use in future works (such as articles or books) all or part of this thesis.

Yun-Hsuan (Stellina) Lee March 24, 2017

High-throughput Whole Ganglion Neural Imaging in *Caenorhabditis elegans* with Microfluidic Systems

by

Yun-Hsuan (Stellina)Lee

Hang Lu

Co-Adviser

Astrid Prinz

Co-Adviser

Neuroscience and Behavioral Biology

Michael Crutcher

Committee Member

Jessica Raper

Committee Member

Kathleen Bates

Committee Member

2017

High-throughput Whole Ganglion Neural Imaging in *Caenorhabditis elegans* with Microfluidic Systems

By

Yun-Hsuan (Stellina)Lee

Hang Lu

Co-Adviser

Astrid Prinz

Co-Adviser

An abstract of
a thesis submitted to the Faculty of Emory College of Arts and Sciences
of Emory University in partial fulfillment
of the requirements of the degree of
Bachelor of Sciences with Honors

Neuroscience and Behavioral Biology

2017

Abstract

High-throughput Whole Ganglion Neural Imaging in
Caenorhabditis elegans with Microfluidic Systems

By Yun-Hsuan (Stellina)Lee

The relationship between neural structure and function at a systemic level is important in understanding how disease affects the brain. Investigation of such implicates pathophysiology of diseases, including neurodevelopmental disorders such as autism spectrum disorder (ASD) and neurodegenerative diseases such as Alzheimer's Disease (AD) and Huntington Disease (HD). Although higher organisms, including mice, Rhesus Macaques, and humans, are very valuable in understanding brain function, the scale and scope of such studies is limited for ethical reasons as well as by monetary resources. In comparison, *Caenorhabditis elegans* is a small nematode that can be cultured isogenically in bulk. It is the only animal model whose nervous system structure has been completely mapped, making localization of function possible. It is also the only organism in which the entire head ganglion, can be simultaneously imaged, capturing different classes of neurons including sensory, motor, and interneurons. This presents a unique opportunity for complete mapping of the relationship between neural structure and function. However, traditional data acquisition and processing approaches are low-throughput, presenting challenges for efficient whole ganglion neural analysis. This thesis thus presents preliminary data enabled by microfluidic devices, introducing an effective method to increase throughput for investigation on neural structure and function.

We interrogate whole ganglion neural properties from two fronts:1) functional imaging of neurons and 2) static imaging of synapses. For functional imaging, we increased

efficiency at both the data acquisition and processing level by acquiring large-scale data with the help of microfluidic devices and through the validation of a developed 3D neuronal tracker. For static imaging, we qualitatively phenotyped the synapses of worms with developmental and genotypic variations. We then quantitatively compared the heterogeneity of neural features that contributes to the formation of a mature functional nervous system through an image processing and statistical analysis pipeline. The two parallel studies highlight the significance of whole ganglion neural imaging in *C. elegans* enabled by microfluidic systems. These initial studies demonstrate the potential for this methodology to inform our understanding of variability in neural structure and function at a systemic level.

High-throughput Whole Ganglion Neural Imaging in *Caenorhabditis elegans* with Microfluidic Systems

By

Yun-Hsuan (Stellina)Lee

Hang Lu

Co-Adviser

Astrid Prinz

Co-Adviser

A thesis submitted to the Faculty of Emory College of Arts and Sciences
of Emory University in partial fulfillment
of the requirements of the degree of
Bachelor of Sciences with Honors

Neuroscience and Behavioral Biology

2017

Acknowledgements

I would like to thank Dr. Hang Lu for continuously supporting and inspiring me throughout my experience in her laboratory. I would like to thank Dr.Charles Zhao, Kathleen Bates, Farhan Kamili, and Shivesh Chaudhary for mentoring me during my research experience. I would like to acknowledge Petit Undergraduate Scholars Research Program for funding my fellowship during 2016 and connecting me to a network of scholars. I would like to acknowledge Dr. Leah Roesch for her support and encouragement throughout the honors program, and my thesis Committee members, Dr. Hang Lu, Dr. Astrid Prinz, Dr. Michael Crutcher, Dr. Jessica Raper, and Kathleen Bates for their constructive feedback in making this thesis possible.

Table of Contents

Abstract

The relationship between neural structure and function at a systemic level is important in understanding how disease affects the brain. Investigation of such implicates pathophysiology of diseases, including neurodevelopmental disorders such as autism spectrum disorder (ASD) and neurodegenerative diseases such as Alzheimer's Disease (AD) and Huntington Disease (HD). Although higher organisms, including mice, Rhesus Macaques, and humans, are very valuable in understanding brain function, the scale and scope of such studies is limited for ethical reasons as well as by monetary resources. In comparison, *Caenorhabditis elegans* is a small nematode that can be cultured isogenically in bulk. It is the only animal model whose nervous system structure has been completely mapped, making localization of function possible. It is also the only organism in which the entire head ganglion, can be simultaneously imaged, capturing different classes of neurons including sensory, motor, and interneurons. This presents a unique opportunity for complete mapping of the relationship between neural structure and function. However, traditional data acquisition and processing approaches are low-throughput, presenting challenges for efficient whole ganglion neural analysis. This thesis thus presents preliminary data enabled by microfluidic devices, introducing an effective method to increase throughput for investigation on neural structure and function.

We interrogate whole ganglion neural properties from two fronts:1) functional imaging of neurons and 2) static imaging of synapses. For functional imaging, we increased efficiency at both the data acquisition and processing level by acquiring large-scale data with the help of microfluidic devices and through the validation of a developed 3D neuronal

tracker. For static imaging, we qualitatively phenotyped the synapses of worms with developmental and genotypic variations. We then quantitatively compared the heterogeneity of neural features that contributes to the formation of a mature functional nervous system through an image processing and statistical analysis pipeline. The two parallel studies highlight the significance of whole ganglion neural imaging in *C. elegans* enabled by microfluidic systems. These initial studies demonstrate the potential for this methodology to inform our understanding of variability in neural structure and function at a systemic level.

Introduction

A major goal of neuroscience research is to examine the relationship between brain structure and function. Brain-wide sampling examines both anatomical connectivity and the activity pattern of neuronal populations (Churchland et al., 2012). Specifically, whole ganglion neural analysis considers neural structure and function at a systemic level, an ideal probe into brain-wide neural dynamics. *Caenorhabditis elegans* is an ideal model organism for studying these dynamics in several ways. First, its optical transparency, compact nervous system, short life cycle, and ease of genetic manipulation makes experiments accessible and feasible (Nguyen et al., 2015). Second, its high genetic homology to humans enables researchers to investigate complex gene-linked human diseases in the much simpler worm (Baumeister & Ge, 2002). Third, it is a powerful model organism for whole ganglion neural imaging. It is complex enough to have all the major tissues including neural, muscular, and somatic, yet simple enough to have its whole nervous system (302 neurons and 8,000 synaptic connections) anatomically mapped and well-characterized (White et al., 1986). Using fine-scale structural information of *C. elegans* nervous system, we can more effectively study how synaptic and neuronal connections contribute to neural function. For example, we can look at how defects in synaptic connectivity contributes to impaired function, or whether certain developmental stages necessitate certain neural structure and thus function (Hodgkin, 2005). The combination of whole ganglion neural imaging and *C. elegans'* well-studied nervous system presents a unique opportunity to pioneer a complete mapping of how neural structure and function relate to one another (Schrödel, 2013). However, traditional approaches rely on manual manipulation of worms and manual data processing, and are thus low-throughput,

prompting this project to employ microfluidic systems for high-throughput imaging and data processing with single-cell resolution. Microfluidic devices (Figure S1A) can be used to overcome the throughput limitations of traditional techniques by allowing us to orient worms in a repeatable fashion and image multiple worms quickly in parallel (Chung, 2008).

The **aim** of this project is to characterize *C. elegans* neural structure and function in a high-throughput fashion by combining whole ganglion neural imaging with microfluidic systems. We interrogate neural properties of *C. elegans* with two parallel studies: 1) Functional imaging of the entire head ganglion to track individual neurons communicating through neural circuitry. 2) Static imaging of a) synaptic morphology during development, and b) synaptic variation with genotypic differences to investigate the heterogeneity of neural features.

1) Functional Imaging

Previous studies in *C. elegans* have shown that behavioral outputs are largely encoded through the collective, dynamic activity of neurons (Alivisatos et al., 2012; Kato et al., 2015). In lieu of traditional views of feed-forward sensory-to-motor pathways, parallel neuronal classes are horizontally organized and interconnected within the neuronal wiring diagram (Prevedel et al., 2014; White et al., 1986). Specifically, these large collections of neurons showed global population dynamics that share a low-dimensional, pervasive neuronal signal, suggesting high-level behavioral organization (Kato et al., 2015). The most salient benefit of using *C. elegans* for functional imaging is the ability to image individual neurons of the entire head ganglion simultaneously and over time. This allows us to track "brain-wide" neural dynamics involved in both active behavior and resting behavior. By using genetically encoded calcium indicators expressed in nuclei pan-neuronally, non-

invasive functional imaging can be conducted via fluorescence microscopy. The development of imaging technology such as light-sheet and light-field microscopy further allows simultaneous, volumetric recordings of large neural tissues for high-throughput and high-content imaging at single-cell resolution (Ahrens et al., 2013). Calcium imaging has thus been used to record whole brain neuron dynamics in vivo in larval *Danio rerio* (zebrafish) brains (Ahrens et al., 2013) and larval *Drosophila* (Lemon et al., 2015) with high spatiotemporal resolution. Whereas whole brain level investigation is challenging in many model organisms, we can visualize the entire head ganglion of *C. elegans* at once (Zhao et al., 2016). Recently, several publications have characterized *C. elegans* neural dynamics at a whole head ganglion level; for example, the high level of correlated activity amongst neuronal groups in response to sensory stimuli or to encode motor outputs. These studies have been done in both freely-behaving (Nguyen et al., 2015; Venkatachalam et al., 2015) and partially anesthetized animals (Schrödel et al., 2013; Prevedel et al., 2014; Kato et al., 2015). However, no paper thus far has examined data for more than five individual worms.

The main bottleneck lies in the data analysis. Traditional analysis requires tracking individual neurons through extensive manual annotation. This is both time- and labor-intensive, which limits statistical power and makes some experiments unfeasible. In particular, variability in neural activity across subjects demands large sample sizes; for example, questions such as which neural populations are involved in commanding motor outputs (Kato et al., 2015), and which microcircuits are involved in response to sensory stimulations (Venkatachalam et al., 2015).

The absence of a high-throughput method for whole brain functional imaging poses an attractive research direction. By facilitating the data processing step, functional imaging

can achieve efficiency and increase throughput for subsequent analysis on larger sample sizes. This portion of my thesis therefore aims to further improve and validate an efficient and automated neuronal tracker, previously developed in the lab of Professor Hang Lu by Dr. Charles Zhao. The neuronal tracker aims to achieve accurate, large-scale automated processing via efficient image processing, effective parameterization, and accurate statistical analysis (Fan et al., 2009). Automated pipelines for neuronal tracking have been documented in mouse models in vivo using 3D optical microscopy (Fan et al., 2009) and neural progenitor cells in stem cell research (Vestergaard et al., 2013). Automating neuronal tracking consistently follows a pipeline consisting of image pre-processing, neuronal tracking, then post-processing. Individual animals exhibit variations in intensity of fluorescent markers; however, this can be resolved with an image processing pipeline that follows segmentation, a registration algorithm, and smoothing consecutively. Segmenting isolates individual neurons in the image, followed by a registration algorithm that tracks the neuron consistently from one frame to another, and finally smoothing mitigates any outliers and random noises during tracking.

The registration algorithm reduces interference of noise, outliers, and missing points by using Coherent Point Drift (CPD), a probabilistic method for non-rigid point set registration that considers individual neurons as points on a deformable volume of space (Myronenko and Song, 2006). We validated the neuronal tracker's tracking accuracy with previous studies (Kato et al., 2015), which in turn enabled us to apply the tracker to large-scale videos we acquired for higher statistical power. Since efficient imaging of hundreds of subjects requires high-throughput data acquisition and processing, microfluidic techniques expedite large-scale global brain imaging data acquisition (Chung et al., 2008). Here, we

increased efficiency for global brain functional imaging research at both the data acquisition and data processing level, inviting future research to investigate systemic neural dynamics in a high-throughput fashion.

2) Static Imaging

In addition to studying neural dynamics and coordination via functional imaging, we investigated synapse structure and function via static imaging. Identification of features such as the intensity and size of synaptic distribution establishes parameters in understanding neural connections that can lead to disease pathology. *C. elegans*' well-understood nervous system has commonly been described as having "stereotypical [positioning] of neurons" and "invariant connectivity" (White et al., 1986). Ample molecular and genetic research has shown a conserved presynaptic compartment structural organization and core synaptic vesicle machinery from *C. elegans* to vertebrates (Richmond, 2005). Nonetheless, little research has addressed how synaptic morphology and plasticity during development contribute to a functional adult nervous system (Jin, 2005). Complications arise due to the significant heterogeneity of distinct neuron types in the central nervous system and the general lack of morphological landmarks for synapse formation (Goda & Davis, 2013; White et al., 1986). We therefore investigate the heterogeneity of synaptic features at each developmental stage, aiming to characterize which features most significantly contribute to trends and variability in synapse formation.

Synapse formation requires two concurrent events *en passant*: 1) the recognition of presynaptic and postsynaptic cells often via recognition signaling and cell adhesion, and 2) synaptic machinery precisely assembled and localized to the synaptic compartments (Cherra & Jin, 2014). The two classes of genes that regulate synapse formation are core

assembly genes and modulator genes. The former one necessitates synapse formation while the latter one modulates synapse morphology, location, or number (Cherra & Jin, 2014). *C.elegans' syd-2* gene is a core assembly gene; the protein it encodes, SYD-2, was the first protein identified as a necessary component of synaptic development (Zhen & Jin, 1999). The SYD-2 protein is the nematode homolog of Liprin-α (Lar-interacting-protein-related)- alpha proteins, and is localized to the presynaptic density. It interacts with upstream modulator and downstream targets to organize active zone formation as a presynaptic signaling scaffold protein (Chia et al., 2013; Dai et al., 2006).

Active zones are plastic structural sites for synaptic vesicle docking and fusion where neurotransmitters are released. The active zone density is highly regulated, with required minimum spacing between neighboring active zones. This finding has been suggested to reflect that synaptic vesicle pools are distributed amongst active zones (Neher, 1998). Thus, each active zone contains equal and sufficient numbers of synaptic vesicles and effective clearance of neurotransmitters ensures synaptic transmission efficacy (Meinertzhagen et al., 1998). Although the morphology of active zones is highly variable within and across species, the architectural organization and machinery is likely to be conserved (Zhai & Bellen, 2004; Burns & Augustine, 1995). In order to visualize presynaptic active zones and the synaptic vesicle pools within those active zones, we use a global pan-synaptic marker strain that co-expresses GFP with the SYD-2 protein under its endogenous promoter.

Active zone formation requires synaptic vesicles; as synapse formation requires precise orchestration of many developmental events including cell migration, axon guidance, and synaptogenesis (Jüttner & Rathjen, 2005), the developmental timescale of

synaptic morphology in *C. elegans* can be a useful tool in understanding synapse development. The *C. elegans* nervous system exhibits various forms of plasticity during development: White et al. (1978) described an intrinsic synaptic re-wiring phenomenon seen in GABAergic Dorsal D (DD) motor neurons. Neurons abolish pre-existing synapses and reform synapses on other sites via reciprocal responsiveness between muscles and motor neurons without changing neuron morphology. As the nematode goes through its four larval stages with a fivefold increase in body length, neurons maintain similar densities of synapses. This implies that there is tremendous plasticity in larval nervous system structure where synaptic formation matches the developmental timeframe of body growth. The spatial-temporal interaction suggests a regulated relative level of plasticity that depends upon *C. elegans* overall growth throughout development (Dabbish & Raizen, 2011).

In addition to studying synaptic morphology during development, synaptic variation due to mutations can provide insight into genomics and human health (Jaramillo-Lambert, 2015). Synaptic variations have been shown to correlate with neurodevelopmental disorders such as autism spectrum disorder (ASD) and schizophrenia (Zoghbi et al., 2012). Synapse losses- in particular- are associated with several debilitating neurodegenerative diseases such as Alzheimer's Disease (AD) and Huntington's Disease (HD) (Kurup & Jin, 2015). *C. elegans'* high genetic homology to humans makes it a prime model for linkage studies relating genotypes to neural phenotypes. Nonetheless, the complex role of localization and regulation of synapses in establishing a functional adult nervous system remain unclear (Goda & Davis, 2013).

Herein, we use a *C. elegans* strain with a global pan-synaptic fluorescent marker expressed in-line with SYD-2 protein, which is localized to the presynaptic active zones. As such, we consider the interaction and interdependencies of synaptic densities and look at synaptic features at a whole ganglion level comparing developmental and genotypic variations. This strain was created by a collaborating lab using the CRISPR-Cas9 gene editing technique; thus, *syd-2* expression is under the control of its natural promoter throughout the entire nervous system. This allows us to quantify expression robustly throughout the head ganglion (Friedland et al., 2013).

Whereas the anatomical structural connectome of *C. elegans* has been fully mapped (White et al., 1986), how synapse formation contributes to the functional connectome has yet to be investigated (Hong & Park, 2016). Moreover, current mapping of synapse formation to the local connectome is mostly at the molecular level (Chia et al., 2013; Cherra & Jin, 2014; Patel et al., 2006). However, to understand the system-level control of neural functions, including behavior, we require systemic-level investigation of neural structure and function (Hong & Park, 2016). This project therefore aims to characterize, for the first time, stereotypical patterns of synaptic features at a whole ganglion level via a global pan-synaptic, endogenous marker strain, from which we will validate existing biological hypotheses and propose novel hypotheses. We hope to extract global synaptic connection information, which will complement the currently mapped connectome with functional relevance of neural connections and wiring (Goda & Davis., 2013).

In sum, my thesis project **aims** to increase efficiency for global brain functional imaging at both the data acquisition and processing level by acquiring large-scale data and validating the developed 3D neuronal tracker. For the static imaging project, we visualized

the following synaptic features of the global pan synaptic marker strain: 1) formation and deterioration of synapses during certain developmental stages of the worm life cycle (Jüttner & Rathjen, 2005) and 2) different synaptic assemblies comparing mutant to wild type strains (Goda and Davis, 2013). We then identified and characterized the global heterogeneity of synaptic features via image analysis. From which, we correlated salient neural features including size and intensity to the formation of a mature functional nervous system via comparisons of developmental and genotypic variations. The parallel studies underscore the need for high-throughput neural imaging to investigate neural structure and function at a whole ganglion level.

Methods

1) Functional Imaging

Whole Head Ganglion Imaging with Microfluidic Systems

All videos (~100) are generated with the *C. elegans* strain ZIM 504 (Genotype: mzmEx199 (Punc-31::NLSGCaMP5K)), which expresses the Ca^{2+} sensor GCaMP5K pan-neuronally in the nucleus (Kato et al., 2015). Worms are temporarily immobilized with 5mM tetramisole solutions prior to being loaded onto a microfluidic device that passively orients worms for a lateral view of the worm (Cáceres et al., 2012; Figure S1B). All recordings occur within two hours of tetramisole rinses. Whole brain imaging videos are recorded under 40x magnification, where each Z stack (20μm), which contains 10 z-planes with 2μm spacing between, is taken under green fluorescence (GFP: 488nm) for 10 minutes (Temporal resolution: 0.576 timepoints/sec). As C*. elegans' n*eurons transmit information via graded potentials that last for several seconds (Liu et al., 2009), the calcium transients from the individual neurons can be effectively captured with the specified time resolution. Data are acquired using an inverted spinning disk confocal microscope (PerkinElmer) equipped with an EMCCD camera (Hamamatsu).

Applying the 3D Neuronal Tracker

The 3D neuronal tracker was previously developed in the lab of Dr. Hang Lu by Charles Zhao (Zhao et al., 2016; Cho et al., 2017). The tracker was coded via Matlab and follows the workflow: segmentation, point set registration tracking, and post-processing. (Figure S2) Each global brain imaging video contains ~320 volumes, each with 10 frames

per volume for a total of ~3200 frames. Each video is processed through the tracking algorithm for a total processing time of approximately two hours per video. The algorithm considers overlay neurons in each volume as well as neuronal movements and intensity change over time (Figure S3).

Validating Accuracy of Neuronal Tracker

Videos from previous studies (Kato et al., 2015) are manually annotated and compared with the tracking data after applying the neuronal tracker. For the manual curation, an individual neuron's trajectory over time is curated manually with consideration of worm shifting and each neuron's relative location to other neurons. The curation repeats for every single neuron recorded from the video and takes up to a week for manual annotation of one video. The neuronal tracker takes ~2hrs of data processing time. To compare tracking accuracy, a Pearson product-moment correlation coefficient (PMCC)/distance criterion followed by Gale-Shapley algorithm (Zhao et al., 2016) is used to validate the neuronal tracker's accuracy. Additionally, we used principal component analysis (PCA) to extract temporal PCs and generate a neural state-manifold. We then compared this manifold to the one generated from hand-curated data. Each temporal principal component (PC) is calculated via the weighted average of the multi-neuron time series (Kato et al., 2015). To increase statistical power of the neuronal tracker's accuracy, the tracker is applied onto the large-sample acquired videos (~100) from this study, and neurons that were wrongly labeled or unidentified are manually annotated.

2) Static Imaging

Preparing worm strains

All strains contain a fusion of SYD-2::GFP, where *syd-2* is a gene that encodes the synaptic assembly scaffolding protein SYD-2. Thus, its endogenous expression is localized to presynaptic active zones. Additionally, SYD-2 has been suggested to play a key role in recruiting presynaptic components, in which *syd-2* mutant exhibits failure of synaptic vesicle accumulation at presynaptic sites, or the active zones (Patel et al., 2006).

a. *Developmental Variation:* 20 worms are imaged at 5 developmental time points post-hatch: Larval stage 1 (L1, 9 hrs), larval stage 2 (L2, 21hrs), larval stage 3 (L3, 29hrs), larval stage 4 (L4, 37hrs), and adults (52hrs) using agarose pad-imaging (White et al., 1978).
b. *Genotypic Variation:* ~10 late L4 worms of each genotype are imaged.
    - Wild type (WT): control group for background presynaptic densities. Genotype: syd-2 (wy (w73(gfp (no introns) :: syd-2)
    - *unc-104* Knockout (KO): The *unc-104* gene makes a protein that is responsible for synaptic vesicle distribution by mediating anterograde axonal transport of synaptic vesicles along axonal microtubules, and is homologous to human kinesin motor protein (Hall et al., 1991; Kumar et al., 2010). The *unc-104* knockout strain used in these experiments lacks this protein. Additionally, it is essential for transporting synaptic precursors to synapses, where SYD-2 is thought to be a cargo of UNC-104 (Yeh et al., 2005; Wagner et al., 2009). We are interested in whether lacking this protein alters active zone distribution at the presynaptic domain. If so, then this strain will exhibit altered synaptic distribution compared to WT.

- *syd-1* (lf): *syd-1* is a gene that makes a protein which downregulates *syd-2* presynaptic components recruitment (Patel et al., 2006). We thus predict that this loss-of-function mutant strain will show an overall decreased intensity of the presynaptic densities.

Imaging Conditions

Agarose pad imaging is used for the developmental variation project and a microfluidic array device (Lee et al., 2014; Figure S4) that enables efficient loading of L4 synchronized population is used for the genotypic variation project. The microfluidic array device is first rinsed with M9 buffer, then worms are loaded onto the device with a pressurizer. All worms are temporarily immobilized with 5mM tetramisole solution prior to loading, and all images are taken within one hour of tetramisole rinse. Data are acquired using an inverted spinning disk microscope (PerkinElmer) equipped with an EMCCD camera (Hamamatsu). Images were taken under 100x magnification, where each Z stack was taken under green and red fluorescence. The regions of interest are whole ganglion presynaptic active zones around the pharyngeal bulb, which are highlighted by GFP. The red channel is used to identify lipid droplets in order to exclude them from being classified as neurons. A bright field image is taken to serve as the reference frame.

Data Analysis

Images are processed and analyzed using Image J (Schneider et al., 2012). For each developmental and genotypic variation group, 1 set of 13 salient features are identified to characterize the stereotypical features of synapses in each group. Quantitative analysis of the 13 synaptic features of interest follows to validate existing biological hypotheses and

propose novel hypotheses. A list of synaptic features of interest for each project is summarized below (Table 1).

Intensity	Area	Single Particle Measurements	Fit Ellipse Measurements	Other
Total Intensity	Total Area	Average size of Active Zones (AZ)	Major Axis	Mass Shift
Normalized Nerve Cord Intensity	Synapse/area ratio	Synapse Intensity Range	Minor Axis	Entropy
		Coefficient of Variation (CV)	Angle	
			Aspect Ratio	

A. 13 Synaptic Features of Interest for Developmental Project.

Intensity	Area	Fit Ellipse Measurements	Other
Total Intensity	Area of Biggest Active Zone (AZ)	Major Axis	Coefficient of Variation (CV)
Normalized Nerve Cord Intensity	Percent area of Biggest Active Zone (AZ)	Minor Axis	Mass Shift
	Total Area	Angle	Entropy
	Perimeter	Aspect Ratio	

B. 13 Synaptic Features of Interest for Genotypic Project.

Table 1. Synaptic Feature List for Each Project

Two sets of synaptic features that were quantified for each developmental (A) and genotypic (B) group. Based on qualitative observation of raw images, we chose salient features that exhibit homogeneous or heterogeneous trend within or between groups.

To measure solely the presynaptic densities in all images, the red channel image is first subtracted from the GFP image to exclude the lipid droplets. To calculate intensity of the presynaptic densities, a large region of interest (ROI) is predefined using the ROI manager tool to mask the area of the biggest active zone (nerve ring). A small ROI is used to mark a selected area of the background intensity to calibrate intensity across images. Total intensity of the presynaptic densities is calculated with the equation: Corrected total fluorescent intensity (CTFI)=Integrated density of the big ROI- (Area × Mean fluorescence of the small ROI). Normalized nerve cord intensity is calculated by normalizing intensity over the length of the nerve cord using the line tool. To calculate entropy, also known as texture or the granularity, a Gray-Level Co-Occurrence Matrix (GLCM) plug-in on Image J was used. The GLCM texture analysis yields an entropy measurement, which considers the spatial relationship of pixels, where higher entropy indicates a coarser image.

To quantify other features such as size and centroid, the images follow the processing pipeline (Figure S5A): detect edges→color threshold (intermodes, exclude edges) →particle analysis. This process segments presynaptic densities into particles, where the biggest particle (biggest active zone) detected overlays with the nerve ring. Equations used to calculate specific features are listed below:

$$Synapse/Area = \ (Total\ Number\ of\ Particles\ Detected)/(Total\ Area)$$

$$Mass\ effect = distance\ (\Delta X\ )between\ centroid\ and\ center\ of\ mass;$$

$$Aspect\ Ratio\ =\ (Major\ Axis)/(Minor\ Axis)\ (Figure\ S5B)$$

$$Synapse\ Intensity\ Range = Maximum - minimum\ gray\ values$$

$$Coefficient\ of\ Variation\ (CV) = Single\ particle\ intensity\ \ \sigma/\mu$$

$$Percent\ Area\ of\ Biggest\ AZ =\ \ (Biggest\ Particle\ detected\ (AZ))/(Total\ Area)$$

Using GraphPad Prism 6.0 (GraphPad Software, Inc., San Diego, CA), a Kruskal-Wallis test followed by Dunn's multiple comparison's test is used to test significant difference of features between the different developmental and genotypic groups. Kruskal-Wallis test is the non-parametric version of one-way ANOVA, but does not assume Gaussian distribution and compares the median of data. This statistical analysis enables more accurate comparison for our sample size and considers highly variable outliers (McDonald, 2014). Principal Component Analysis (PCA) follows to reduce features dimensions and explain within-group, between-subject variations using the Excel add-in Multibase package (Numerical Dynamics, Japan). To compare the variance of the features within each genotypic or developmental group, within-group coefficient of variation (CV) is calculated with the formula: σ/μ. A normalized total CV is subsequently calculated: For each feature, the percentage of CV for each group is calculated. The normalized percent CV is then added up across each group for a normalized total CV that accounts for the 13 features. The within-group CV measures variability of each feature within-group, and allows us to elucidate the heterogeneity of synaptic features that correlates with specific developmental stage or genotype.

Results

1) Functional Imaging

Initially, we imaged worms on agar pad to acquire videos of functional activity. However, most videos produced inconsistent data due to incorrect worm orientation. As worm orientation is crucial for downstream processing, we started using a microfluidic device (Figure S1) that controls for worm orientation while standardizing imaging conditions. Controlling the worm orientation to a lateral side view allows us to visualize neurons, including overlapping neurons, from the dorsal to ventral side of the worm. The use of microfluidic systems thus streamlines and expedites whole brain functional imaging at the data acquisition level by increasing throughput (~100 videos). Functional imaging data shows that individual neurons exhibit differential activity over time, even during resting state. (Figure 1). We applied the 3D neuronal tracker (Zhao et al., 2016; Figure S2) to the

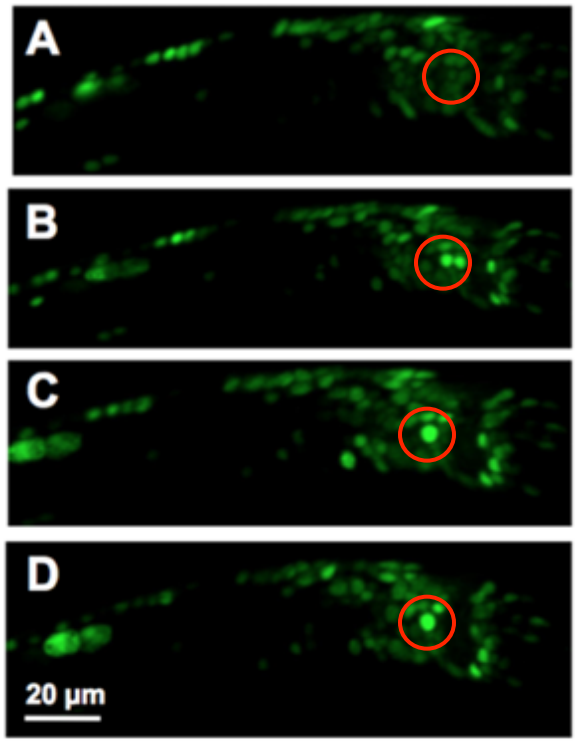

Figure 1: Functional imaging

Representative functional imaging on four different time points for a specific video is shown. Figure 1A-D shows simultaneous recording of the whole head ganglion. Intensity in the green channel indicates calcium levels in neurons, and red circles denote group of neurons with time-varying activity.

videos, where each video returned ~120 neurons tracked, which is more than 1/3 of all neurons in the worm. We produced a map of the activity of individual neurons over time by plotting the fluorescence intensity as a function of time, which detailed spatiotemporal information of the intensity of each tracked neuron at a specific time point. Neurons close to each other on the y-axis tend to be physical neighbors, but are essentially arbitrary. At a global level, the collective activity of multiple neurons shows that neuronal communication takes place both locally and distally, suggesting dynamic coordination of neuronal populations (Figure 2). These data suggest some possible collective excitatory and inhibitory neuronal communication between neurons both temporally and spatially, which

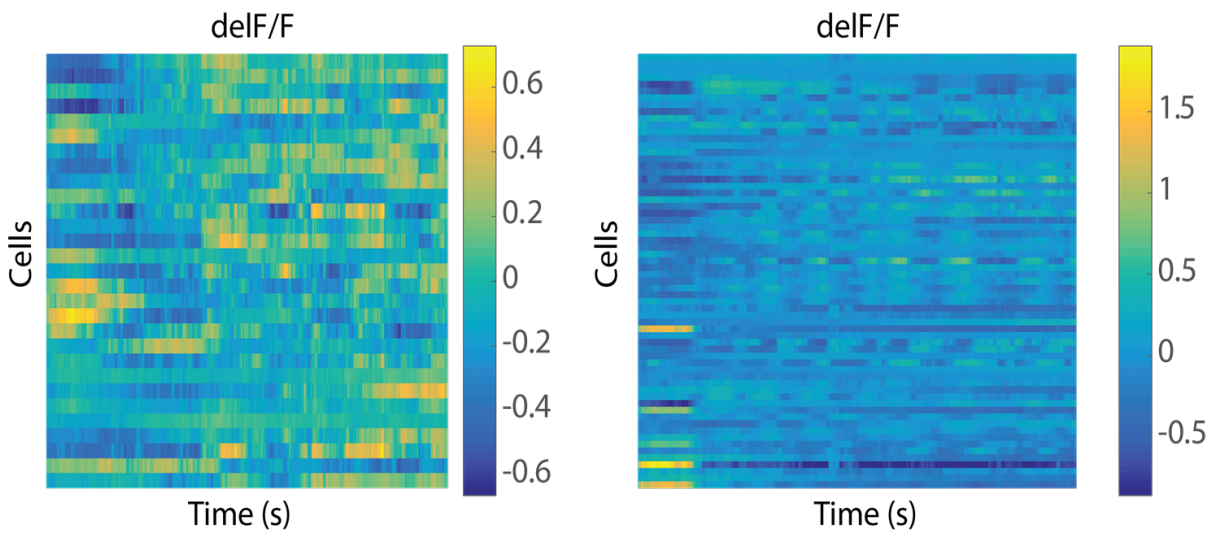

Figure 2: Dynamic Coordination of Collective Neurons

Representative multi-neuron time series where discernable Ca^{2+} activity is seen. Y-axis denotes each neuron (cell) tracked, X-axis denotes the 10-minute timeframe, and each block (delF/F) denotes each neuron's intensity change of green fluorescent traces, with yellow indicating highest intensity and purple the lowest intensity. (Left) ~30 of the most active neurons are chosen from (Right) the full intensity map.

requires larger sample size to validate this hypothesis. The temporal interaction would suggest high-level organization of neuronal outputs that dictate a temporal window for active neuronal classes (Kato et al., 2015), whereas spatial interaction would suggest horizontal communication within or between neuron classes (Prevedel et al., 2014; White et al., 1986). We applied the neuronal tracker to videos acquired from previous studies (Kato et al., 2015) and compared the neurons tracked and their fluorescent trace intensities. We manually curated (~6) of Kato's videos by tracking each individual neuron one by one (Kato et al., 2015). We validated the accuracy by Pearson product-product-moment correlation coefficient (PMCC)/distance criterion followed by a Gale-Shapley algorithm (Zhao et al., 2016). Our PMCC value of 0.97 was close to a total positive correlation of 1; this demonstrates the neuronal tracker's (our data) comparable accuracy to manual curation (Kato's Data) (Figure 3A, Zhao et al., 2016; Kato et al., 2015). Consistently, neural-state manifolds via principal component analysis (PCA) on the time derivatives of the calcium normalized traces show similar results between our data and Kato's data, where global oscillation in neural activity is seen. Temporal principal components represent a low dimensional representation of temporal activity of neurons. This is achieved by clustering activities of individual neurons based on their correlations. Few temporal components capture most of the variance in data suggesting collective activity of neurons. The first three temporal PCs show the neural state trajectory on neural-state manifolds (Figure 3B, Zhao et al., 2016; Kato et al., 2015). As the neuronal tracker shows comparable tracking accuracy while significantly enhancing efficiency to 2 orders of magnitude (~2 hours with 3D neuronal tracker vs. up to a week by manual curation), automated processing of whole ganglion videos can achieve throughput for large-scale data

processing. After validating the tracker with videos from previous studies, we applied the neuronal tracker to videos acquired from the current study and manually annotated cells that were wrongly labeled or unidentified. This step is crucial as it helped established the tracker's consistency amongst different videos. We calculated the percentage of frames with erroneous cells for each cell (tracking error percentage) and summed the number of cells for each tracking error percentage. The neuronal tracker returned high accuracy, where minimal errors are found and most errors are readily detected. (Figure 3C). Together, these findings introduce a high-throughput method for whole ganglion functional neural imaging at both the data acquisition and processing level.

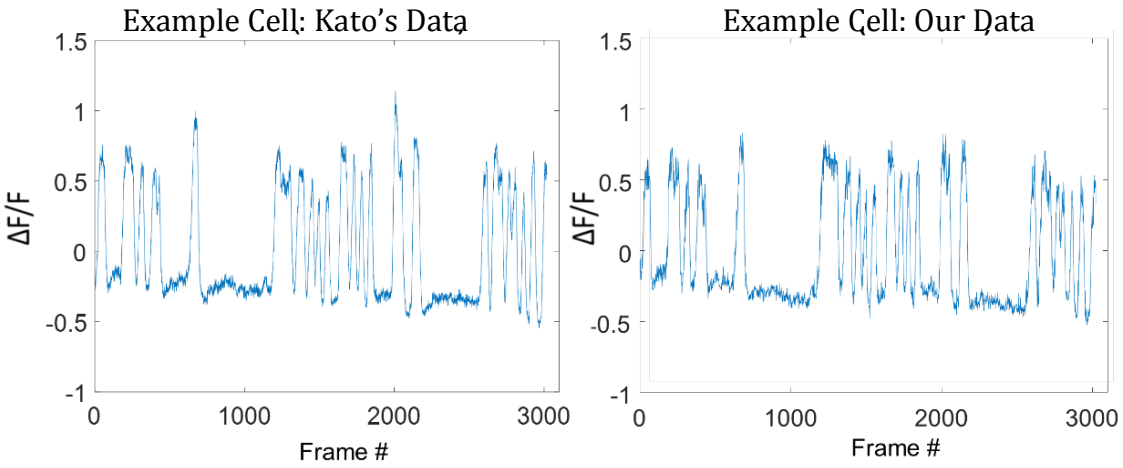

A.

Pearson's Product-Moment Correlation Coefficient (PMCC):0.97

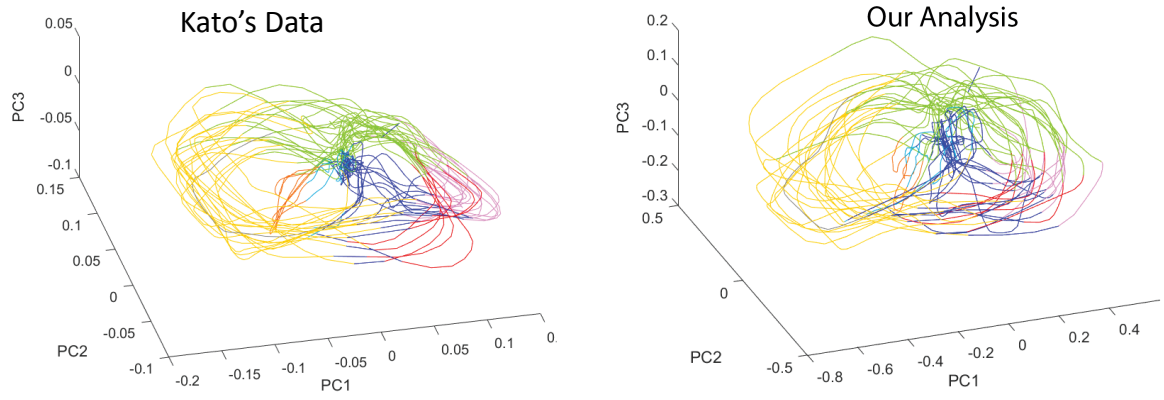

B.

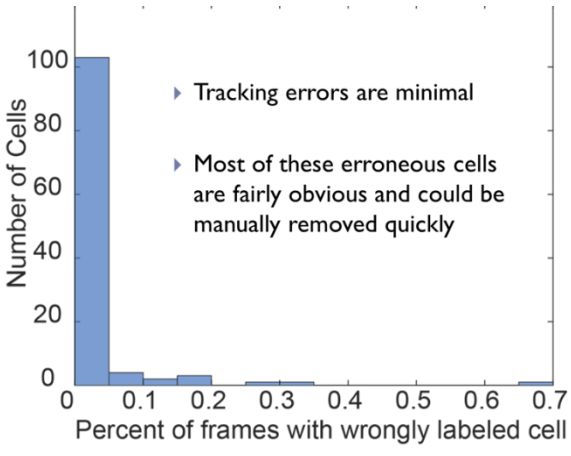

C.

Figure 3: Validation of tracking accuracy

A. Comparison of tracking data using a PMCC/distance criterion followed by Gale-Shapley algorithm. ΔF/F denotes intensity change of green fluorescent traces. Median PMCCs for the 6 videos: 0.71-0.76, and median distance: 2.4-10.5 pixels. B. Similar neural-state manifolds via Principal Component Analysis (PCA). C. Tracking Error Rate by cell on videos acquired from the present study.

2) Static Imaging

Static imaging on the synapses of the whole head ganglia shows changes in synaptic morphology throughout development. Synapse formation requires precise orchestration of developmental events at each stage (Jüttner & Rathjen, 2005). Qualitatively, synapses appear around the nerve ring before the L1 stage and reach full growth by L4 (Figure 4A). When the nematode reaches adulthood, synaptic deterioration can be seen (Toth et al., 2012; Figure 4A). Using Image J, we quantified 13 salient features in the worm's head ganglia across each stage of development (Table 1). Whereas total area of presynaptic densities increases throughout the 5 stages of development with a relative decrease at the L4 stage (not significant), the overall intensity remains constant (Figure 4B, upper), consistent with previous findings where synapses maintain similar spacing with neighboring synapses during development and expand area with physical growth (Dabbish & Raizen, 2011). This independence of synaptic intensity from the developmental timeframe suggests that synaptogenesis occurs on a timescale that parallels physical growth, reflective of a spatial-temporal interaction. Therefore, developmental timeframe is necessary, yet not sufficient alone, for synapse development and formation. Increased trend of entropy (Figure 4B, lower left) throughout the 5 developmental stages suggests more synaptic size variations with increased age that contributes to a coarser image. Therefore, increased number of synapses growing at different rates throughout development contributes to the increased entropy trend. As for mass shift, calculated by the distance between centroid and center of mass to characterize synaptic distribution, no significance was found at significance level $\alpha=0.05$. This is most likely due to our small sample size combined with the high variability on data with a small numerical range; we

therefore decreased the confidence interval to 90% (significance level: α=0.1) to examine whether any general trend exists. Interestingly, mass shift (Figure 4B, lower right) shows an increased trend of active zone movement and distribution with development, with a considerable dip at stage L4. The remarkable decrease here, and the slight decrease from total area suggests L4 as an important development checkpoint. We hypothesize that as the nematode's nervous system is well established at late-L4 stage (White et al., 1986), decreased synaptic growth and distribution might start occurring at early L4 stages. We note that while our small sample size did not yield significant difference between comparison of every developmental stage, the general trend seen in our data is promising for statistical significance with increased statistical power.

We sought to explain whether the different features identified for each developmental stage covaried or whether specific features contributed more at specific stages. We therefore conducted Principal Component Analysis, and found that the variations across the 13 features identified can be reduced to two principal components that account for 89.0% of the variations. Features that contributed most significantly to Principal Component (PC)1 and PC2 include intensity, particle count/area, texture, and CV. Notably, these are features that correlate with particle intensity values, which supports our data and previous studies where synaptic vesicles maintain specified spacing with neighboring synapses during development (Dabbish & Raizen, 2011). The concentric ellipses suggest that presynaptic vesicles exhibit similar properties and trends throughout development, with increased heterogeneity at certain stages. We traced the outliers to their respective raw data and found that the high variability in Adult and L1 was mainly due to high variability of total area of the presynaptic vesicles (Figure 4C). An explanation could

be that more variability occurs during initial synaptic growth when synapses begin to form (L1) and again during synaptic deterioration (Adult). Synapse deterioration around the nerve ring has been characterized as an age-dependent morphological change in *C. elegans* (Toth et al., 2012); the heterogeneity in synaptic growth and deterioration thus can contribute to the large variation in total area. To further characterize the heterogeneity of features within each developmental group, we calculated the within-group coefficient of variation (CV) (Figure 4D). The markedly low CV for intensity suggests the invariability of synaptic formation that parallels physical growth throughout development, and the low CV seen in entropy suggests a stereotypical pattern of synapse size to number ratio at each stage. The entropy reflects the granularity of the segmented particles, a similar granularity of images seen in each stage thus points to similar numbers of particles with the same sizes. In contrast, the high CV of total area indicates high variability for subjects of the same developmental stage. Since *syd-2* gene is a core assembly gene that governs synaptic assembly (Zhen & Jin, 1999), the high CV of total area suggests that the presynaptic assembly machinery is activated for development, yet does not govern the precise timeframe for synaptic spatial pattern. This finding supports current understanding of variable sizes seen in *C. elegans* synaptic regions (Jin, 2005; Zhai & Bellen, 2004). The relatively high CV seen in mass shift, together with the moderately high levels of fit ellipse features such as major, minor, angle, and aspect ratio, point to the heterogeneity of synaptic distribution. This finding suggests that synaptogenesis entails expression of synapses, but not specific synaptic patterns or distributions during development. Notably, the normalized total CV exhibit a U-shaped curve, where inter-subject variability is most high in L1 and adult, and lowest in L3. This finding is consistent with our hypothesis that

more variability or plasticity occurs during initial synaptic growth (L1) and again during synaptic deterioration (Adult) (Figure 4E). These preliminary findings lead to some interesting observations that validate the image processing and statistical processing pipeline, yet require increased statistical power in the future to confirm these hypotheses.

A.

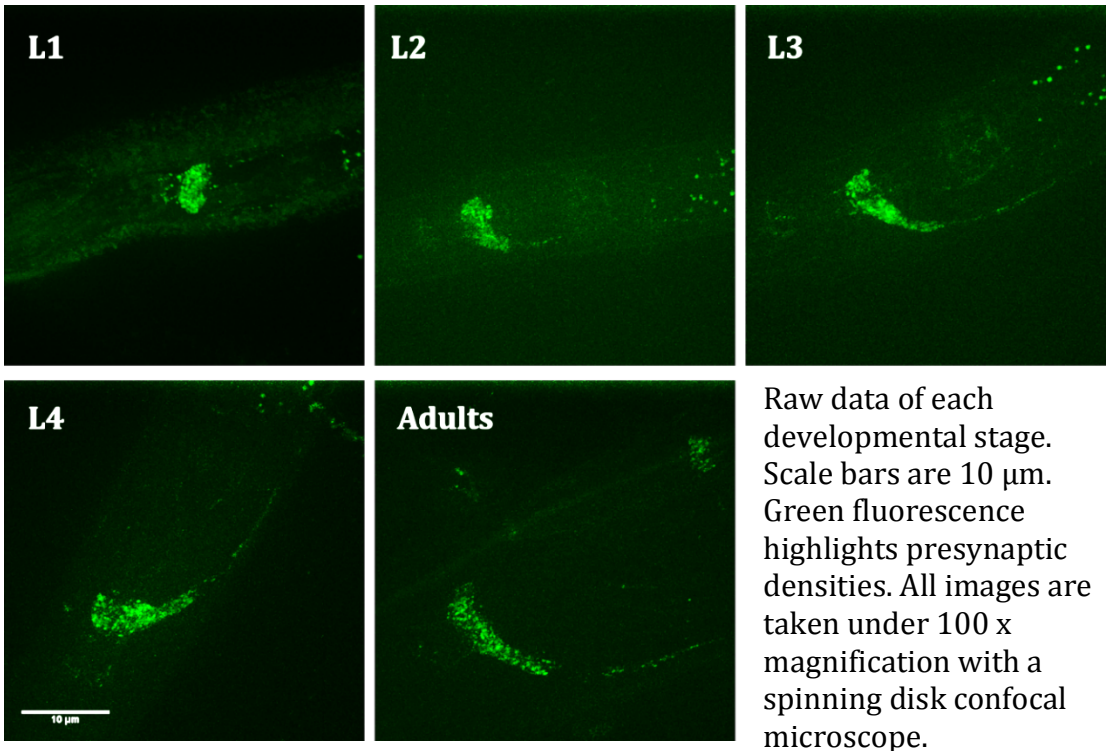

Raw data of each developmental stage. Scale bars are 10 µm. Green fluorescence highlights presynaptic densities. All images are taken under 100 x magnification with a spinning disk confocal microscope.

B.

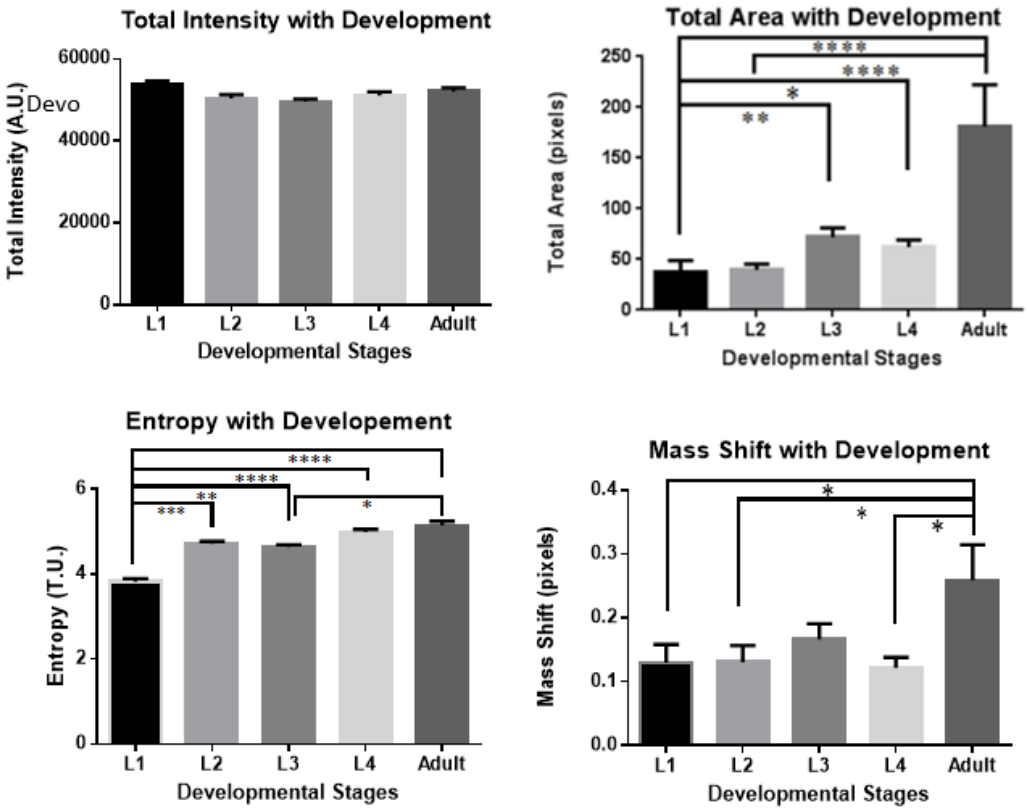

C.

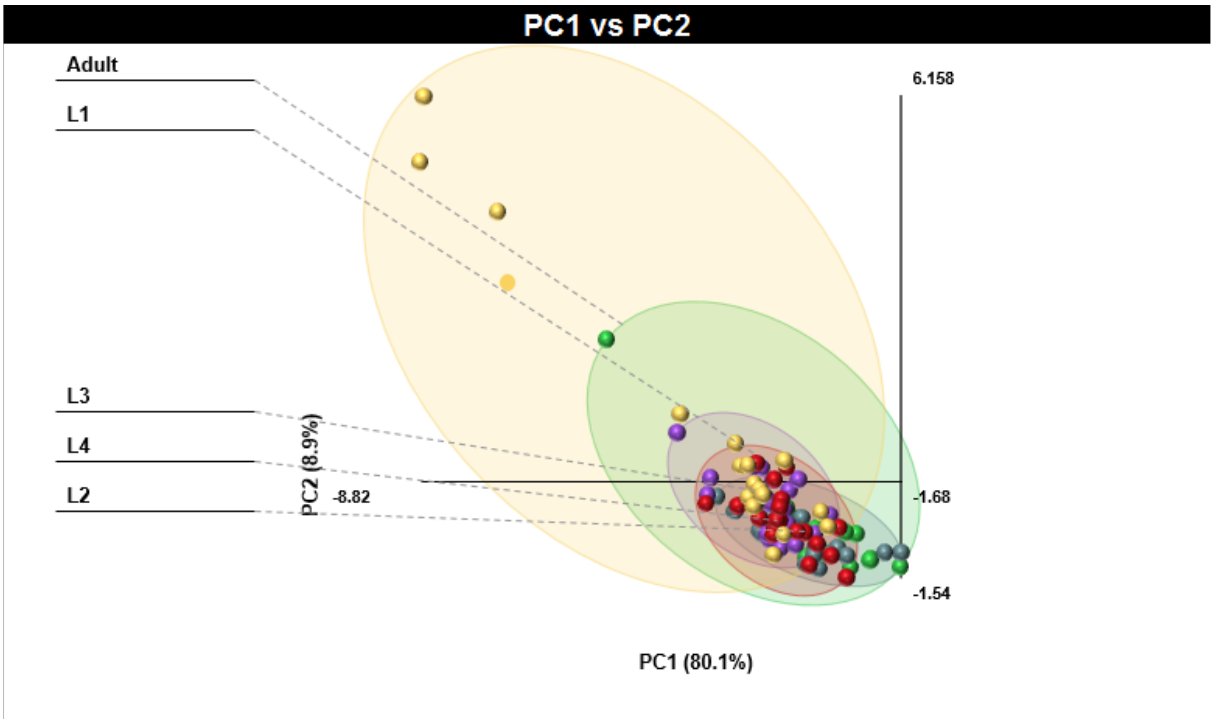
PC1 vs PC2
Adult
L1
L3
L4
L2
6.158
-1.68
-1.54
-8.82
PC2 (8.9%)
PC1 (80.1%)

D.

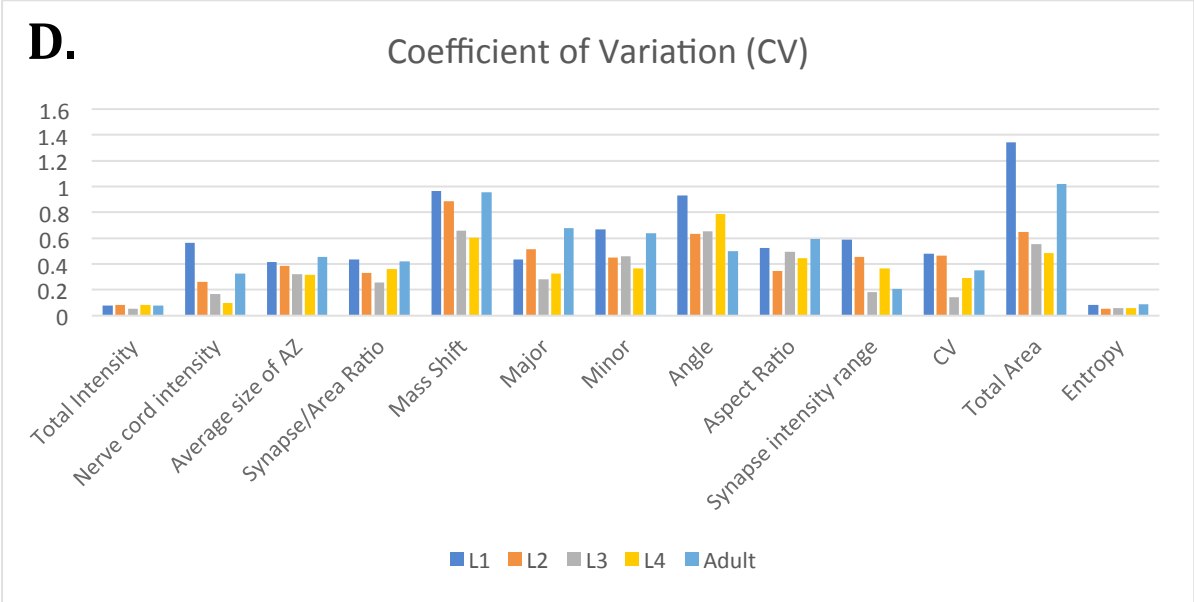
Coefficient of Variation (CV)
1.6
1.4
1.2
1
0.8
0.6
0.4
0.2
0
Total Intensity
Nerve cord intensity
Average size of AZ
Synapse/Area Ratio
Mass Shift
Major
Minor
Angle
Aspect Ratio
Synapse intensity range
CV
Total Area
Entropy
L1
L2
L3
L4
Adult

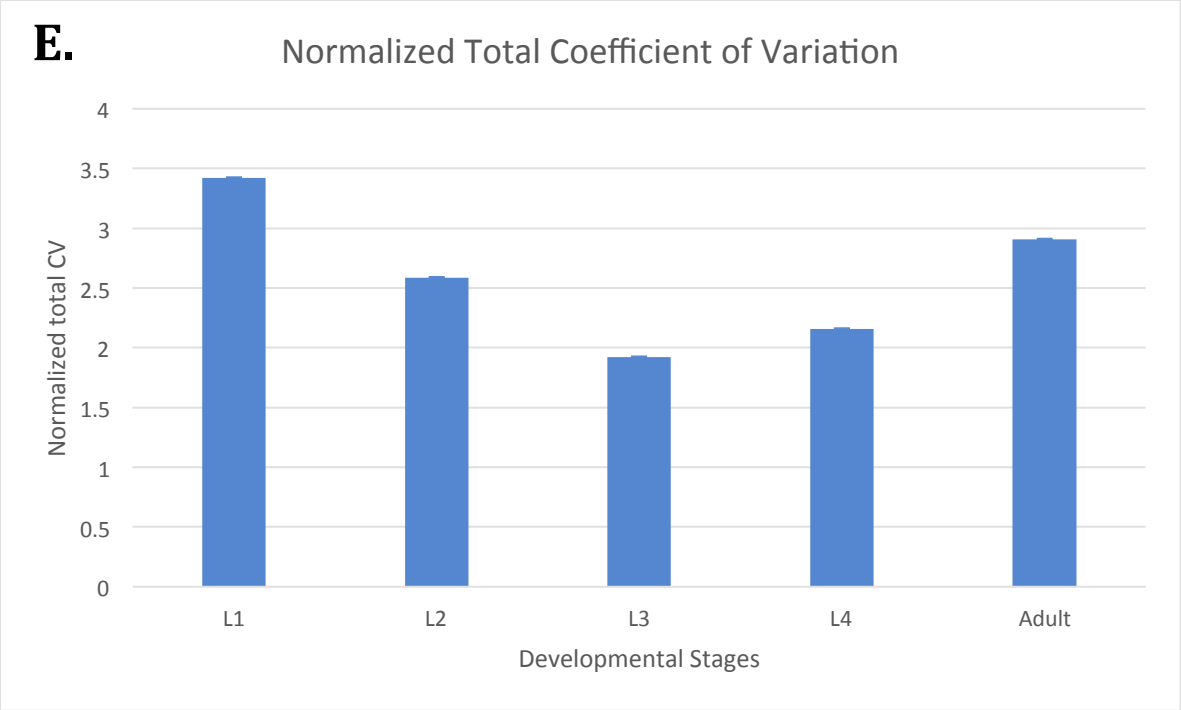

Figure 4. Static Imaging on Presynaptic Vesicles with Developmental Variation

A) Representative qualitative synaptic morphology during the 5 developmental stages B) Kruskal-Wallis Comparison followed by Dunn's post-hoc multiple comparison test in features (n=20 for each developmental stage). Intensity is quantified by Arbitrary Units (A.U.); Entropy is quantified by Texture Units (T.U.). Each bar denotes mean +SEM. Significance level is represented by asterisks. Total Intensity, total area, entropy: Family wise significance level: $\alpha=0.05$, $p \leq 0.05$ (*), $p \leq 0.01$ (**), $p \leq 0.001$ (***), $p \leq 0.0001$ (****); Mass Shift: $\alpha=0.1$, $p \leq 0.1$ (*) C) Principal Component Analysis to reduce feature dimensions D) Within-group Coefficient of variation (CV) for each feature. A high CV indicates high within-group variation that reflects high heterogeneity. E) Normalized total Coefficient of Variation (CV) for each developmental stage considering all features. Each bar denotes sum of normalized CV +SEM.

For the static imaging of synapses on genotypic variations, we observed distinctive neural phenotypes in mutant's synaptic distribution and intensity. For all genotypes, synaptic vesicles cluster into densities at the presynaptic sites, or active zones, as opposed to freely scattered in the cytoplasm. To observe whether lacking UNC-104's anterograde transport function affects SYD-2 presynaptic recruitment to the active zone, we compared our preliminary data to our prediction of *unc-104* (KO)'s altered synaptic distribution. Qualitatively, the *unc-104* (KO) strain exhibited an altered presynaptic active zone distribution, whereas the *syd-1* mutant strain exhibited lower intensity overall (Figure 5A). Kruskal-Wallis test followed by post-hoc Dunn's multiple comparison (Family wise significance level: $\alpha=0.05$) shows that a similar total area, but a significantly smaller percent area of biggest active zone was seen in *unc-104* (KO) compared to WT, suggesting that *unc-104* (KO)'s impairment is not with synaptic formation, but with synaptic distribution (Figure 5B, upper). Since *unc-104* encodes a protein that mediates anterograde transport of synaptic components, the primary synaptic defect for loss of *unc-104* is the failure to transport synaptic vesicles along the axon (Hall et al., 1991; Kumar et al., 2010). This seems to affect SYD-2 presynaptic recruitment to the active zone, thus an altered synaptic distribution was seen in *unc-104* (KO). Interestingly, whereas no significant difference was observed in the normalized nerve cord intensity, a significant increase was seen in total intensity of *unc-104* (KO) compared to WT (Figure 5B, lower). The similar normalized nerve cord intensities, once more, suggests intact synaptic formation of *unc-104* (KO). Together with our qualitative comparison of WT and *unc-104* (KO) (Figure 5A), the increased intensity and a smaller percent area of biggest synaptic active zone reflect aggregation of presynaptic densities approximately halfway between the two pharyngeal

bulbs, where the nerve ring nuclei lie (White et al., 1986). We hypothesize that lacking UNC-104 protein results in failure to transport presynaptic vesicles, leading to increased aggregation at the cell bodies region. Confirmation of aggregation at the nerve ring nuclei would require a marker that highlights the cell bodies in addition to the presynaptic density. Overall, these findings suggest that lack of the *unc-104* impairs synaptic transportation and hence the altered synaptic docking of presynaptic vesicles. As the transportation of synaptic vesicles occur after synaptogenesis, our preliminary data suggest that the UNC-104 protein results in a neural phenotype that exhibits intact synapse formation, but mislocalized synaptic distribution.

The *syd-1* mutant, on the other hand, exhibits altered synapse formation in addition to impaired synaptic distribution. The decreased normalized nerve cord intensity and total intensity (Figure 5B, lower) supports our prediction, as *syd-1* encodes a protein that downregulates *syd-2* presynaptic component recruitment (Patel et al., 2006). We also observed a decreased total area in *syd-1* mutant, likely to reflect synaptic formation defect as well (Figure 5B, upper). Failure to recruit presynaptic component, most importantly, the presynaptic vesicles, results in impaired synaptogenesis. The impaired synapse formation attributes to the altered downstream synaptic distribution, as less synaptic vesicles are recruited to be transported. The fact that the area of biggest active zone (Figure 5B upper) did not differ significantly between *unc-104* (KO) and *syd-1* mutant reflects that failure of synaptic transport can result in a similar presynaptic vesicle docking pattern. Whether these altered patterns share a similar mechanism to perform alternative functions behaviorally requires functional analyses of these linkage studies.

Principal Component Analysis on genotypic variation shows that variations across the 13 features can be best explained by 2 principal components which account for 94.2% of the variations (Figure 5C). Features of WT and *unc-104* (KO) share similar model spaces, manifesting that an altered synaptic distribution is a subset of the WT features, though with different magnitude. In contrast, features of *syd-1* (mutant) occupies a distinctive cluster than that of WT and *unc-104* (KO), confirming that impaired synaptic assembly and downstream transportation results in a distinct neural phenotype. Further analysis on the features contributing to each principal component reveals that the features that most heavily contributed to the first principal component include fit ellipse measures, intensity, and entropy, features that most strongly correlate with synapse distribution.

To characterize the homogeneity of each genotype group, inter-subject coefficient of variation (CV) was calculated for each feature (Figure 5D). Low values of CV in intensity and fit ellipse measurements reflect a rather stereotypical pattern of synaptic distribution within each group. The low CV values for fit ellipse measurements were not seen in the developmental project, suggesting that synaptic distribution perhaps show the most homogenous trends within-group at late L4 stage, as all subjects for the genotypic project were a late L4 stage. One explanation might be that the nervous system is well established at late-L4 stage (White et al., 1986) and that extensive synaptic deterioration has not initiated. In contrast, the high levels of CV for size measurements such as total area, area of biggest AZ, and perimeter suggest that despite the stereotypical synaptic distribution, heterogeneous presynaptic vesicle growth rates are observed. This finding, once again, validates the current understanding of variable presynaptic region in *C. elegans* (Jin, 2005; Zhai & Bellen, 2004). A lower normalized total coefficient of variation was seen in *unc-104*

(KO) compared to WT and *syd-1* mutant, suggesting that synaptic vesicle transportation might contribute to higher variability. Together, these data suggest that both developmental and spatial information contribute to synapse formation and transportation, which in turn results in differential neural phenotypes. These preliminary findings are interesting and require further studies to validate these hypothesis with increased statistical power.

A.

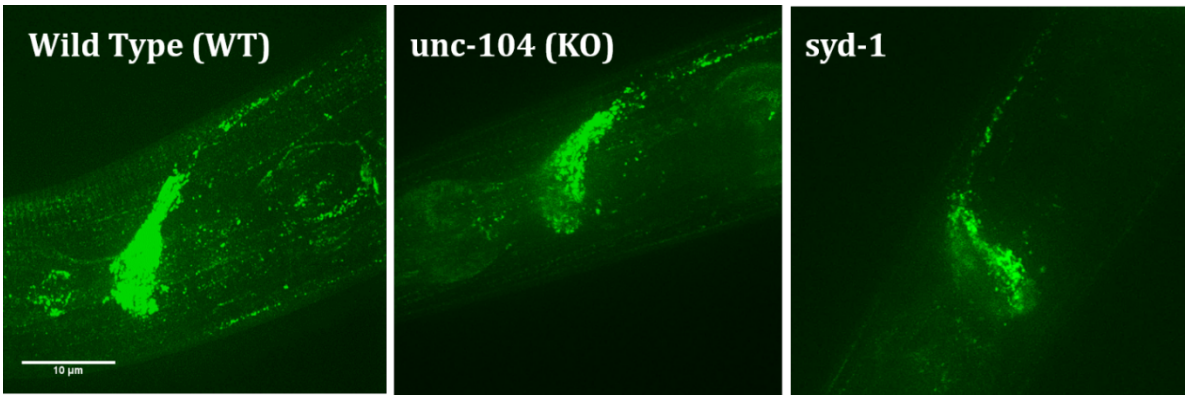
Wild Type (WT)
unc-104 (KO)
syd-1
10 µm

B.

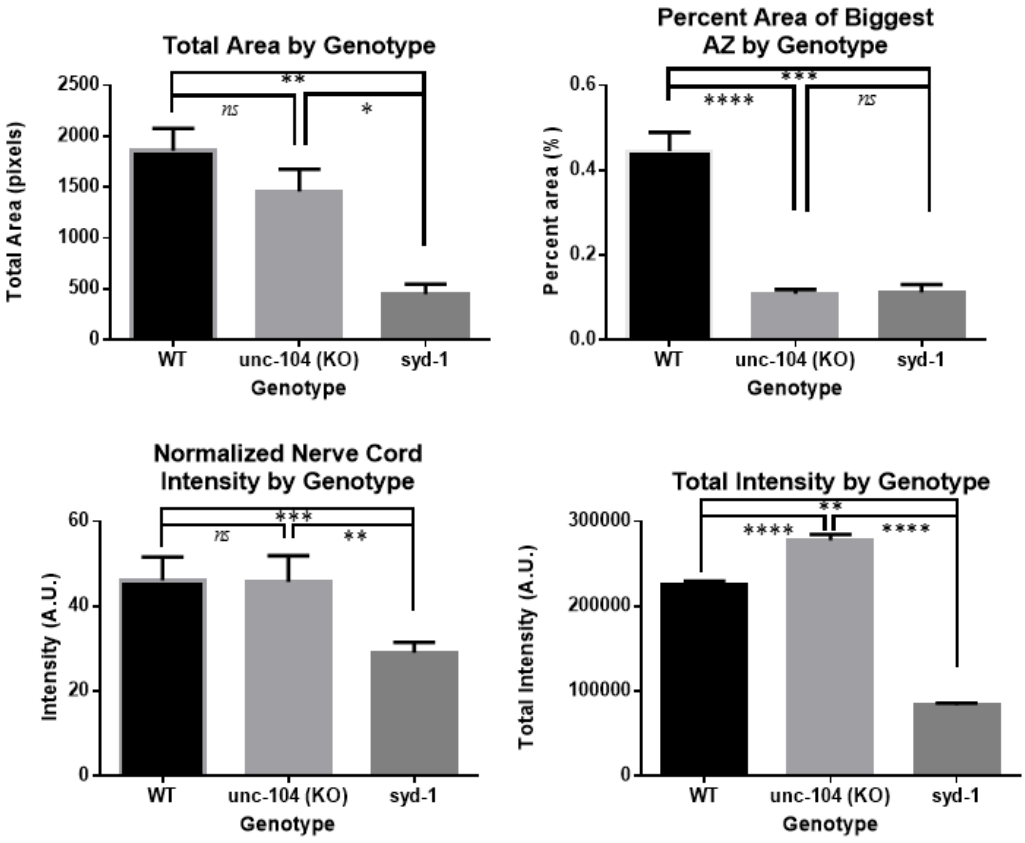
Total Area by Genotype
Total Area (pixels)
2500
2000
1500
1000
500
0
**
ns
*
WT
unc-104 (KO)
syd-1
Genotype
Percent Area of Biggest AZ by Genotype
Percent area (%)
0.6
0.4
0.2
0.0
***
****
ns
WT
unc-104 (KO)
syd-1
Genotype
Normalized Nerve Cord Intensity by Genotype
Intensity (A.U.)
60
40
20
0
***
ns
**
WT
unc-104 (KO)
syd-1
Genotype
Total Intensity by Genotype
Total Intensity (A.U.)
300000
200000
100000
0
**
****
****
WT
unc-104 (KO)
syd-1
Genotype

C.

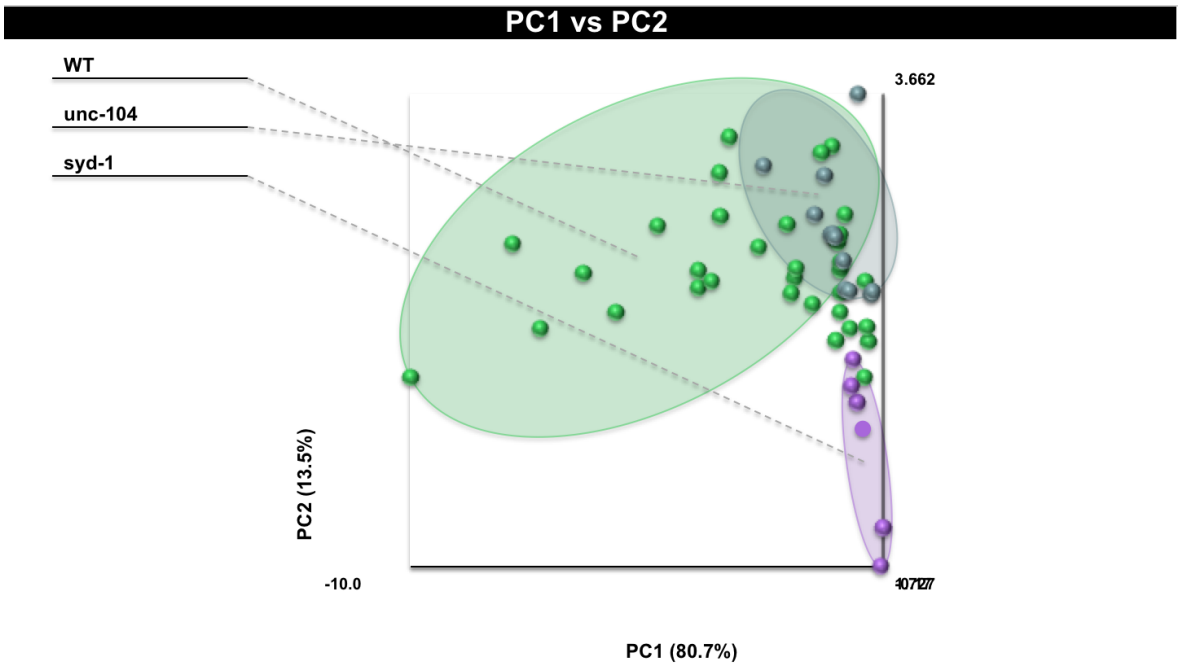
PC1 vs PC2
WT
unc-104
syd-1
3.662
-10.0
PC2 (13.5%)
PC1 (80.7%)

D.

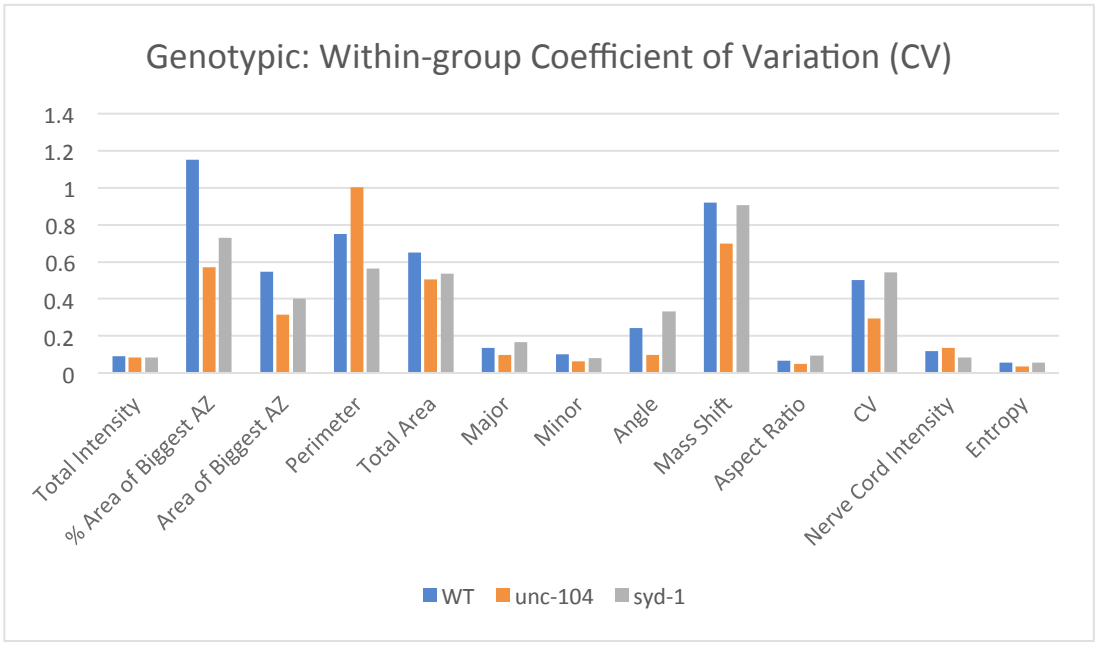
Genotypic: Within-group Coefficient of Variation (CV)
1.4
1.2
1
0.8
0.6
0.4
0.2
0
Total Intensity
% Area of Biggest AZ
Area of Biggest AZ
Perimeter
Total Area
Major
Minor
Angle
Mass Shift
Aspect Ratio
CV
Nerve Cord Intensity
Entropy
WT
unc-104
syd-1

E.

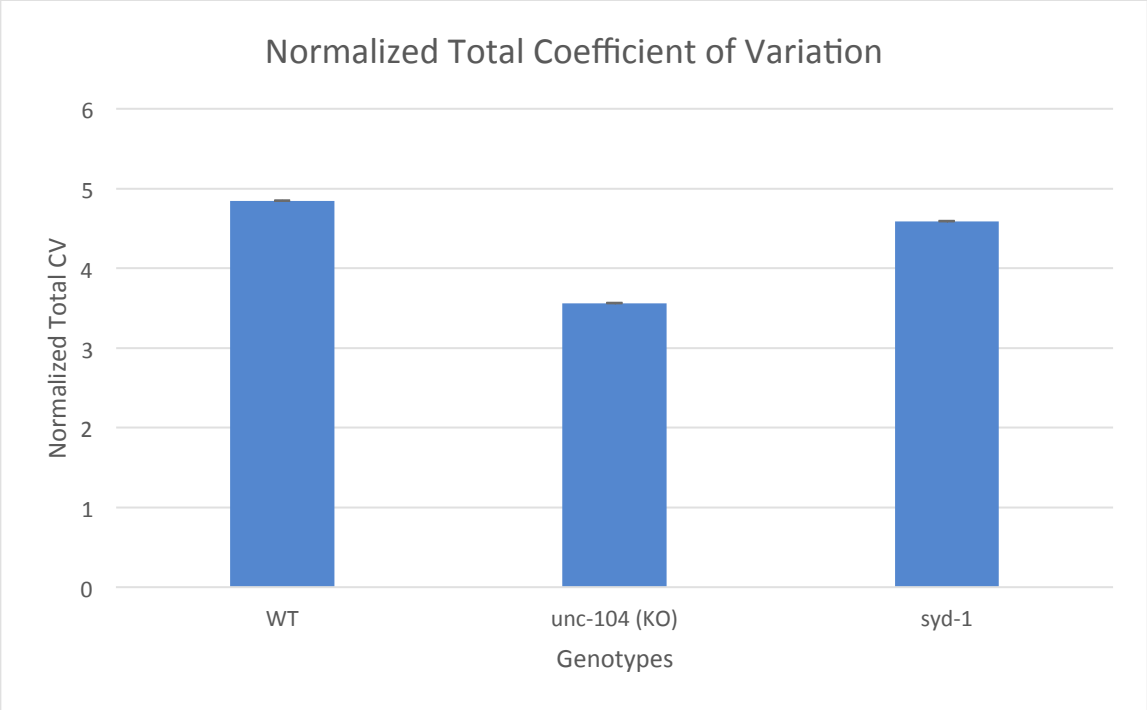

Figure 5. Static Imaging on Presynaptic Active Zones with Genotypic Variation

A) Representative qualitative neural phenotypes with 3 different genotypic strains. B) Kruskal-Wallis Comparison followed by Dunn's post-hoc multiple comparison test in features (WT: N=33; *unc-104* (KO): N=11; *syd-1* (mutant): N=6) Intensity is quantified by Arbitrary Units (A.U.). Each bar denotes mean +SEM. Significance level is represented by asterisks. Family wise significance level: $\alpha=0.05$, $p \leq 0.05$ (*), $p \leq 0.01$ (**), $p \leq 0.001$ (***), $p \leq 0.0001$ (****); ns: no significance. C) Principal Component Analysis show different color clusters of neural features based on genotypes. Green: WT; Yellow: *unc-104* (KO); Purple: *syd-1* (mutant) D) Within-group Coefficient of Variation (CV) for each feature E) Normalized total Coefficient of Variation (CV) for each developmental stage considering all features Each bar denotes sum of normalized CV +SEM.

Discussion & Conclusion

For both functional and static imaging, combining microfluidic devices and whole ganglion neural imaging facilitates high-throughput data acquisition, which introduces efficiency for investigation of neural circuitry and synaptic features. By validating the developed 3D neuronal tracker with additional functional imaging videos, we increased efficiency at both the data acquisition and processing level for future analysis of neural circuitry structure and function. For the static imaging project, we qualitatively and quantitatively described the heterogeneity of neural features both within and between groups of developmental and genotypic variation. We characterized, via a global pan-synaptic marker strain, presynaptic densities of *C. elegans'* at the whole ganglion level, gaining insight into synapse formation and its spatial-temporal dependency.

We employed 2 different microfluidic devices for different experimental measures. For functional imaging, we used a device that controls worm orientation so that the calcium traces are recorded from the lateral side of the worms. Our animals were anesthetized in the imaging chamber; imaging on sensory-stimulated or freely-behaving animals would require more complex systems. For example, a sensory stimulus channel could be connected to the imaging valve of the current microfluidic device for a chemosensory stimulation study (Cho et al., 2017). Alternatively, an imaging system with automatic re-centering followed by neuronal traces reconstruction to process 3D, simultaneous calcium transients (Ngyuen et al., 2015; Venkatachalam et al., 2015) can be employed for studies on freely behaving animals. For the static imaging project on genotypic variation, we employed a worm array that holds up to 140 worms, which enables large sample size screenings of worms of the same age (L4). During imaging, however, one important

consideration is the worm orientation (dorsal/ventral vs. lateral). For quantitative analysis, images with consistent worm orientation were chosen, yet many were discarded. Therefore, a device that allows for large sample loading while controlling for worm orientation can be developed for a more efficient data acquisition. Additionally, the current device is designed only for the L4 age, therefore, it might be worthwhile to develop devices that enable efficient feature phenotyping of all other life stages. The high-throughput data acquisition highlights the advantage of using microfluidic devices to streamline experimental conditions.

Another complication during imaging is the varied intensity of each imaging session due to environmental factors or microscopy settings. For example, the developmental and genotypic variation project was taken under different microscopy settings, hence the distinctly different intensity values. To address this issue, fluorescent microspheres can be used to calibrate the fluorescent intensities during each imaging session and between each imaging subject (Wu et al., 2007). The varied intensity due to environmental factors seen in raw data can be addressed with data processing. For example, for functional imaging, intensity traces of individual neurons are calculated on a relative scale of change in intensity (ΔF) over initial intensity level (F). The intensity for the static imaging project considers background intensity and normalizes the nerve ring and nerve cord intensity against the background. Since each of the 3 projects, (1) functional, (2) static: developmental, and (3) static: genotypic, were imaged under the same microscopy setting, we were able to compare data within each project without microspheres calibration. However, in order to compare across projects, such as one that compares which

developmental stage is critical before pathological synaptic variation occurs, fluorescent microspheres can be employed.

1) Functional Imaging

We introduced a high-throughput method for whole ganglion functional neural imaging both at the data acquisition and data processing level. From validating the neuronal tracker with previous data and new data, we observed collective activities of neurons that suggest dynamic coordination of neural dynamics. To connect to the well-studied neural connectivity of *C. elegans,* functional imaging videos can be mapped to the neuroanatomical atlas by manual matching (Prevedel et al., 2015; Schrödel et al., 2013). Putative neuron IDs can be reconstructed by considering neurons' anatomical positions and their relative positions to surrounding neurons as well as associating typical activity patterns to specific neurons. To confirm ambiguous neuron identities, Kato et al. (2015) imaged a strain that expressed red fluorophores in the neurons of interest along with the calcium indicator GCaMP5K. Moreover, they used an infrared (IR) camera to track the neuron of interest while simultaneously recording calcium activity. Future research on associating individual neurons detected from the videos to specific neuronal identities in the neuroanatomical atlas deserves attention.

One limitation of using a nuclear localized calcium indicator is our restriction to detect somatic calcium transients, and not subcellular calcium signals. Yet, some neurons in *C. elegans* exhibit subcellular level signal processing via specific neuronal processes (Venkatachalam et al., 2015; Li et al., 2014; Hendricks et al., 2012). However, collective neuronal populations encode dynamic activity as represented by the neural state

manifolds, despite possible distinct subcellular signals. Future research can aim at how similar and distinct subcellular signals contribute to the collective activity of specific neuronal populations for specific functional outputs.

Our functional imaging was conducted on animals anesthetized and confined to a restricted space. Freely behaving animals (Nguyen et al., 2015; Venkatachalam et al., 2015) or animals not anesthetized can potentially uncover more prominent neural patterns. Even so, we observed distinctive neural patterns from collective neuronal populations. We hypothesize that these neuronal signals might encode information that pertains to the discrepancy between high-level organizational outputs and downstream motor confinement. In other words, the nematodes desire to move but are unable to due to immobilization. This introduces opportunities for whole ganglion functional imaging with various experimental manipulations, potentially uncovering specific circuitry responsible for specific behavior at a systemic level. For example, whether stimulating specific body parts of the nematode or presenting different food choices can elicit activation of differential neural circuitries (Zaslaver et al., 2015); or whether multisensory integration to modulate locomotor behavior is governed by hierarchal neural organization (Cho et al., 2017; Summer et al., 2015) could be studied. Furthermore, all videos from this study were recorded for 10 minutes. Longer timescales on functional imaging can potentially unveil characteristic neural patterns that influence brain states such as sleep/wake cycle (Raizen et al., 2008) or hunger/satiety states (You et al., 2008).

One other interesting area would be to manipulate neural activity and observe the resulting behavior. Optogenetic manipulations to activate specific neurons (Shipley et al.,

2014) or neuropeptides to inhibit neurotransmission (Laurent et al., 2015) can be conducted to observe the relationship between whole ganglion neural dynamics and behavioral outputs. For example, optical activation of mechanosensory neurons can result in altered motor outputs (Shipley et al., 2014); whether activation of those specific neurons triggers communication within the class-specific hierarchical organization or between the horizontal pathways of neural networks propose a fascinating research direction.

2) Static Imaging

For static imaging, we used a global pan-synaptic marker strain that highlights the presynaptic densities. We then qualitatively and quantitatively characterized synaptic features that contribute to a mature functional nervous system. Despite a humble sample size due to unforeseen complications in transgenic strain maintenance, we observed stereotypical patterns for different groups with developmental or genotypic variation, and characterized the general heterogeneity within-group. Through quantitative analyses of synaptic features, we derived interpretations of synapse formation and distribution that pertain to specific developmental stage or mutations. We validated existing biological hypotheses and proposed novel hypotheses, and identified synaptic features that contribute to a mature and functional nervous system. By examining within-group coefficient of variation (CV) and conducting principal component analysis (PCA) for all features, we identified the neural features that most robustly distinguish one group from another. These preliminary data serve as a basis to understand the variability in synaptic formation and distribution at different developmental stages or with different genotypic

variation, which will inform our understanding of neural structure and function at a global synaptic level.

One dilemma that we encountered with static imaging was the balance between high resolution imaging (100x) that captures the entire nerve ring, or lower resolution (10x, 40x) that captures the entire nerve ring and the nerve cord. We chose the former one as we are interested in characterizing *C. elegans*' whole head ganglia, and because high resolution (100x) under the spinning disk microscopy effectively captured a fine spatial resolution of the nerve ring. One future direction can be to capture all of the synapses of a single worm by taking multiple images along the entire worm body, enabling characterization of the synaptic vesicles localized to the active zones at an organismal level.

With regards to our quantitative analysis, the image processing program we used, ImageJ, segmented synaptic vesicles localized to the active zones into particles that represent multiple synapses. A more precise segmentation of current images, or images with higher spatial resolution of the nerve ring, can possibly detect individual synapses and trace synapse formation and migration at a finer scale. Furthermore, rotation of the subjects can result in detection of variable areas of synaptic vesicles. One way to address this limitation is by using a microfluidic device that controls for both the worm orientation and the alignment of multiple worms at once.

When studying developmental variation in synaptic morphology, we observed a general stereotypical growth of presynaptic densities, but high variation between subjects at each developmental stage. While this finding supports the considerable variance in presynaptic regions between *C. elegans* (Jin, 2005), another consideration is that the

temporal scale of the nematode's nervous system development is even finer. We imaged subjects at a specified hour during each developmental stage; yet, as we can observe differences in images between early L4 and late L4 stages by comparing developmental (early L4) and genotypic variations (later L4); thus, perhaps a finer timescale will deepen our current understanding of synapse development. An interesting future direction could be conducting long-term time-lapse imaging on this global pan-synaptic strain, which could allow observation of how synapses are formed and how synaptic vesicles are transported on a finer timescale.

From looking at genotypic variation of synapses, we characterized differences in synaptic formation and distribution between the mutant strains compared to the wildtype. As synaptic variations and synapse losses implicate neurodevelopmental and neurodegenerative disorders (Kurup & Jin, 2015; Zoghbi et al., 2012), synaptic variation comparison via the simple nematode nervous system can be advantageous in unveiling pathological factors. We specifically conducted linkage analysis on two mutant strains with impaired synaptic vesicle transportation and impaired synaptic component recruitment, respectively. While increased statistical power is required to associate synaptic impairments specific to genes, our data serves as a preliminary finding for future investigation. To further understand the timescale of pathological synaptic formations and distributions, future studies can aim at characterizing neural features of the mutant strains during development. For the *unc-104* (KO), since our strain only highlights the presynaptic vesicles localized to the active zones and not the cell bodies, we hypothesized that the aggregation of presynaptic vesicles at the estimated anatomical position of the nerve ring nuclei (White et al., 1986) was due to the failure of presynaptic vesicle transportation.

However, a marker that highlights both the cell bodies and presynaptic density is needed to confirm this hypothesis. Alternatively, time-lapse static images can be taken at fine temporal resolution to track the synaptic vesicle distribution during development.

Overall, the two parallel studies in this thesis underscore the significance of the high-throughput whole ganglion neural imaging enabled by microfluidic systems. Through functional imaging of neural dynamics and static imaging of synapses, we investigated neural properties at a systemic level, gaining insight into neural structure and function. The homogeneity and heterogeneity in neural features presents future directions of pursuing imaging at higher spatial or temporal resolution. In this thesis we have shown that whole ganglion neural imaging combined with the advantages of microfluidic systems allows a greatly increased throughput that will be significant in future neuroscience research.

References:

Ahrens MB, Orger MB, Robson DN, Li JM, Keller PJ (2013) Whole-brain functional imaging at cellular resolution using light-sheet microscopy. Nature Methods 10:413–420.

Alivisatos ACAP, Chun M, Church GM, Greenspan RJ, Roukes ML, Yuste R (2012) The Brain Activity Map Project and the Challenge of Functional Connectomics. Neuron 74:970–974.

Baumeister R, Ge L (2002) The worm in us – Caenorhabditis elegans as a model of human disease. Trends in Biotechnology 20:147–148.

Burns ME, Augustine GJ (1995) Synaptic structure and function: dynamic organization yields architectural precision. *Cell* 83: 187–194.

Cáceres IDC, Valmas N, Hilliard MA, Lu H (2012) Laterally Orienting C. elegans Using Geometry at Microscale for High-Throughput Visual Screens in Neurodegeneration and Neuronal Development Studies. PLoS ONE 7.

Cherra SJ, Jin Y (2014) Advances in synapse formation: forging connections in the worm. Wiley Interdisciplinary Reviews: Developmental Biology 4:85–97.

Chia PH, Patel MR, Wagner OI, Klopfenstein DR, Shen K (2013) Intramolecular regulation of presynaptic scaffold protein SYD-2/liprin-α. Molecular and Cellular Neuroscience 56:76–84.

Cho Y, Zhao CL, Lu H (2017) Trends in high-throughput and functional neuroimaging in Caenorhabditis elegans. Wiley Interdisciplinary Reviews: Systems Biology and Medicine.

Chung K, Crane MM, Lu H (2008) Automated on-chip rapid microscopy, phenotyping and sorting of C. elegans. Nature Methods 5:637–643.

Churchland MM, Cunningham JP, Kaufman MT, Foster JD, Nuyujukian P, Ryu SI, Shenoy KV (2012) Neural population dynamics during reaching. Nature.

Dabbish NS, Raizen DM (2011) GABAergic Synaptic Plasticity during a Developmentally Regulated Sleep-Like State in C. elegans. Journal of Neuroscience 31:15932–15943.

Dai Y, Taru H, Deken SL, Grill B, Ackley B, Nonet ML, Jin Y (2006) SYD-2 Liprin-α organizes presynaptic active zone formation through ELKS. Nature Neuroscience 9:1479–1487.

Fan J, Zhou X, Dy JG, Zhang Y, Wong STC (2009) An Automated Pipeline for Dendrite Spine Detection and Tracking of 3D Optical Microscopy Neuron Images of In Vivo Mouse Models. Neuroinformatics 7:113–130.

Friedland AE, Tzur YB, Esvelt KM, Colaiácovo MP, Church GM, Calarco JA (2013) Heritable genome editing in C. elegans via a CRISPR-Cas9 system. Nature Methods 10:741–743.

Goda Y, Davis GW (2003) Mechanisms of Synapse Assembly and Disassembly. Neuron 40:243–264.

Hall DH, Hedgecock EM (1991) Kinesin-related gene unc-104 is required for axonal transport of synaptic vesicles in C. elegans. Cell 65:837–847.

Hendricks M, Ha H, Maffey N, Zhang Y (2012) Compartmentalized calcium dynamics in a C. elegans interneuron encode head movement. Nature.

Hodgkin J. Introduction to genetics and genomics (September 6, 2005), WormBook, ed. The C. elegans Research Community, WormBook, doi/10.1895/wormbook.1.17.1

Hong J-H, Park M (2016) Understanding Synaptogenesis and Functional Connectome in C. elegans by Imaging Technology. Frontiers in Synaptic Neuroscience 8.

Jaramillo-Lambert A, Fuchsman AS, Fabritius AS, Smith HE, Golden A (2015) Rapid and Efficient Identification of Caenorhabditis elegans Legacy Mutations Using Hawaiian SNP-Based Mapping and Whole-Genome Sequencing. G3: Genes|Genomes|Genetics 5:1007–1019.

Jin Y. Synaptogenesis (2005), WormBook, ed. The C. elegans Research Community, WormBook, doi/10.1895/wormbook.1.44.1, http://www.wormbook.org.

Jüttner R, Rathjen FG (2005) Molecular analysis of axonal target specificity and synapse formation. Cellular and Molecular Life Sciences 62:2811–2827.

Kato S, Kaplan HS, Schrödel T, Skora S, Lindsay TH, Yemini E, Lockery S, Zimmer M (2015) Global Brain Dynamics Embed the Motor Command Sequence of Caenorhabditis elegans. Cell 163:656–669.

Kumar J, Choudhary BC, Metpally R, Zheng Q, Nonet ML, Ramanathan S, Klopfenstein DR, Koushika SP (2010) The Caenorhabditis elegans Kinesin-3 Motor UNC-104/KIF1A Is Degraded upon Loss of Specific Binding to Cargo. PLoS Genetics 6.

Kurup N, Jin Y (2015) Neural circuit rewiring: insights from DD synapse remodeling. Worm 5.

Laurent P, Soltesz Z, Nelson GM, Chen C, Arellano-Carbajal F, Levy E, Bono MD (2015) Decoding a neural circuit controlling global animal state in C. elegans. eLife 4.

Lee H, Kim SA, Coakley S, Mugno P, Hammarlund M, Hilliard MA, Lu H (2014) A multi-channel device for high-density target-selective stimulation and long-term monitoring of cells and subcellular features in C. elegans. Lab Chip 14:4513–4522.

Lemon WC, Pulver SR, Höckendorf B, Mcdole K, Branson K, Freeman J, Keller PJ (2015) Whole-central nervous system functional imaging in larval Drosophila. Nature Communications 6:7924.

Li Z, Liu J, Zheng M, Xu XS (2014) Encoding of Both Analog- and Digital-like Behavioral Outputs by One C. elegans Interneuron. Cell 159:751–765.

Liu Q, Hollopeter G, Jorgensen EM (2009) Graded synaptic transmission at the Caenorhabditis elegans neuromuscular junction. Proceedings of the National Academy of Sciences 106:10823–10828.

McDonald JH (2014) Handbook of Biological Statistics .3rd ed. Baltimore: Sparky House Publishing, Maryland.

Meinertzhagen I, Govind C, Stewart B, Carter J, Atwood H (1998) Regulated spacing of synapses and presynaptic active zones at larval neuromuscular junctions in different genotypes of the fliesDrosophila andSarcophaga. The Journal of Comparative Neurology 393:482–492.

Myronenko, AX, Song B, Carreira-Perpinan MA (2006). Non-rigid point set registration: Coherent point drift. NIPS 1009–1016.

Neher E (1998) Vesicle Pools and Ca2 Microdomains: New Tools for Understanding Their Roles in Neurotransmitter Release. Neuron 20:389–399.

Nguyen JP, Shipley FB, Linder AN, Plummer GS, Liu M, Setru SU, Shaevitz JW, Leifer AM (2015) Whole-brain Calcium Imaging with Cellular Resolution in Freely Behaving Caenorhabditis Elegans. Proceedings of the National Academy of Sciences USA 07110.

Patel MR, Lehrman EK, Poon VY, Crump JG, Zhen M, Bargmann CI, Shen K (2006) Hierarchical assembly of presynaptic components in defined C. elegans synapses. Nature Neuroscience 9:1488–1498.

Prevedel R, Yoon Y-G, Hoffmann M, Pak N, Wetzstein G, Kato S, Schrödel T, Raskar R, Zimmer M, Boyden ES, Vaziri A (2014) Simultaneous whole-animal 3D imaging of neuronal activity using light-field microscopy. Nature Methods 11:727–730.

Raizen DM, Zimmerman JE, Maycock MH, Ta UD, You Y-J, Sundaram MV, Pack AI (2008) Lethargus is a Caenorhabditis elegans sleep-like state. Nature 453:952–952.

Richmond J. (2005) Synaptic function. WormBook. 1-14

Schneider CA, Rasband WS, Eliceiri KW (2012) NIH Image to ImageJ: 25 years of image analysis. Nature Methods 9:671–675.

Schrödel T, Prevedel R, Aumayr K, Zimmer M, Vaziri A (2013) Brain-wide 3D imaging of neuronal activity in Caenorhabditis elegans with sculpted light. Nature Methods 10:1013–1020.

Shipley FB, Clark CM, Alkema MJ, Leifer AM (2013) Simultaneous optogenetic manipulation and calcium imaging in freely movingC. elegans.

Summers PJ, Layne RM, Ortega AC, Harris GP, Bamber BA, Komuniecki RW (2015) Multiple Sensory Inputs Are Extensively Integrated to Modulate Nociception in C. elegans. Journal of Neuroscience 35:10331–10342.

Toth ML, Melentijevic I, Shah L, Bhatia A, Lu K, Talwar A, Naji H, Ibanez-Ventoso C, Ghose P, Jevince A, Xue J, Herndon LA, Bhanot G, Rongo C, Hall DH, Driscoll M (2012) Neurite Sprouting and Synapse Deterioration in the Aging Caenorhabditis elegans Nervous System. Journal of Neuroscience 32:8778–8790.

Venkatachalam V, Ji N, Wang X, Clark C, Mitchell JK, Klein M, Tabone CJ, Florman J, Ji H, Greenwood J, Chisholm AD, Srinivasan J, Alkema M, Zhen M, Samuel ADT (2015) Pan-neuronal Imaging in Roaming Caenorhabditis Elegans Proceedings of the National Academy of Sciences USA 113.8

Vestergaard JS, Dahl AL, Holm P, Larsen R (2013) Pipeline for Tracking Neural Progenitor Cells. Medical Computer Vision Recognition Techniques and Applications in Medical Imaging Lecture Notes in Computer Science:155–164.

Wagner OI, Esposito A, Kohler B, Chen C-W, Shen C-P, Wu G-H, Butkevich E, Mandalapu S, Wenzel D, Wouters FS, Klopfenstein DR (2009) Synaptic scaffolding protein SYD-2 clusters and activates kinesin-3 UNC-104 in C. elegans. Proceedings of the National Academy of Sciences 106:19605–19610.

White JG, Albertson DG, Anness MA (1978) Connectivity changes in a class of motoneurone during the development of a nematode." Nature 271(5647): 764-766.

White JG, Southgate E, Thomson, JN, Brenner S (1986) The structure of the nervous system of the nematode Caenorhabditis elegans." Philosophical Transactions of the Royal Society B: Biological Sciences 314, 1–340

Wu Y, Campos SK, Lopez GP, Ozbun MA, Sklar LA, Buranda T (2007) The development of quantum dot calibration beads and quantitative multicolor bioassays in flow cytometry and microscopy. Analytical Biochemistry 364:180–192.

Yeh E, Kawano T, Weimer RM, Bessereau JL, Zhen M (2005) Identification of genes involved in synaptogenesis using a fluorescent active zone marker in Caenorhabditis elegans. J Neurosci 25:3833–3841.

You Y-J, Kim J, Raizen DM, Avery L (2008) Insulin, cGMP, and TGF-β Signals Regulate Food Intake and Quiescence in C. elegans: A Model for Satiety. Cell Metabolism 7:249–257.

Yuille AL, Grzywacz NM (1988) A computational theory for the perception of coherent visual motion. Nature 333:71–74.

Zaslaver A, Liani I, Shtangel O, Ginzburg S, Yee L, Sternberg PW (2015) Hierarchical sparse coding in the sensory system ofCaenorhabditis elegans. Proceedings of the National Academy of Sciences 112:1185–1189.

Zhao C, Cho Y, Zimmer M, Lu H (2016) 3D Tracking of Neurons for Whole Brain Imaging in Awake C. elegans with Point Registration.” CeNeuro 2016& Nagoya BNC symposium, July 27-30, 2016, Nagoya, Aichi, Japan.

Zhai RG, Bellen H (2004) The Architecture of the Active Zone in the Presynaptic Nerve Terminal. Physiology 19:262–270.

Zhen M, Jin Y (1999) The liprin protein SYD-2 regulates the differentiation of presynaptic termini in C. elegans. Nature 401:371–375.

Zoghbi HY, Bear MF (2012) Synaptic Dysfunction in Neurodevelopmental Disorders Associated with Autism and Intellectual Disabilities. Cold Spring Harbor Perspectives in Biology 4

Appendices

Figure S1: Microfluidic Device

A. 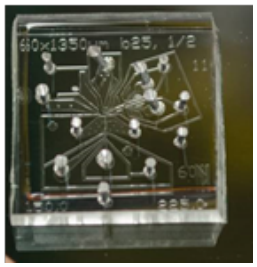

An example microfluidic device is depicted. The dimensions are 1cm x 1cm x 0.4 cm. Microfluidic devices are microchannels molded out of polydimethylsiloxane (PDMS), and can be designed with specific features for large-scale, efficient genomic screening and data acquisition (Chung, 2008).

B. 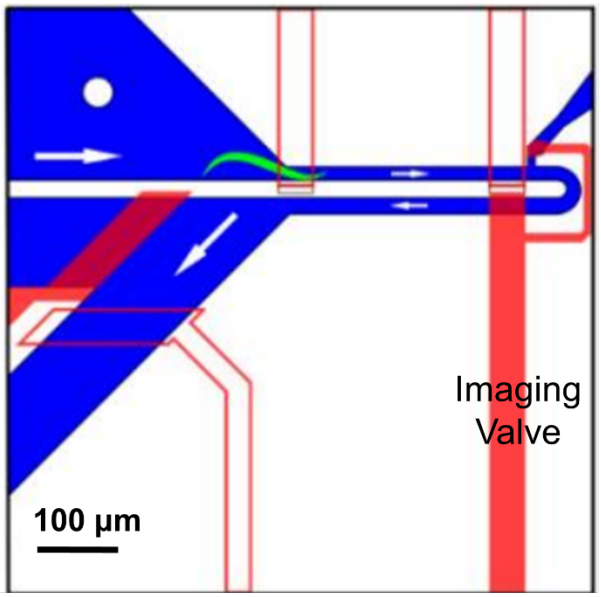

A microfluidic device that controls for worm orientation is depicted. The microfluidic device is designed with a curved worm channel that laterally aligns animals, followed by a straight elongation of the channel immediately after the curve to maintain the worm's straight body posture during imaging (Cáceres et al., 2013). Adult worms that carried 0~4 eggs were used (strain ZIM 504; genotype: Genotype: mzmEx199 (Punc-31::NLSGCaMP5K).

Figure S2: Workflow of the 3D Neuronal Tracker (Zhao et al., 2016)

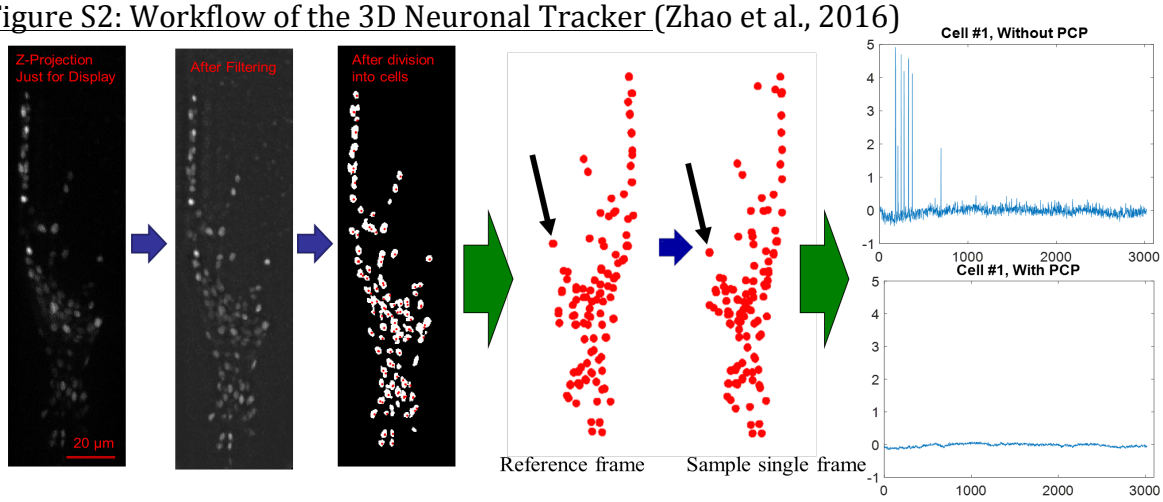

Segmentation → Point Set Registration → Post-Processing

For the pre-processing part, big blobs are first subdivided into individual neurons, Using a Laplacian of Gaussian filter, the maximum projection of individual neurons are segmented out from each frame. Following pre-processing, a point set registration algorithm is used to track and match the neurons in each frame to a well-chosen reference frame (Myronenko & Song, 2006). The data is then smoothed by Principal Component Pursuit , where sparse noise in the calcium traces caused by inaccurate neuronal tracking is mitigated (Candes et al., 2011). A Gale-Shapley algorithm is employed to find occasional missing points by distance, where neurons with high variances in centroids are filtered out.

Figure S3: Applying the neuronal tracker to the video

After applying the neuronal tracker to the video recording (left), neuronal activity of multiple neurons in the head ganglia can be simultaneously tracked through 3D volume recordings (right).

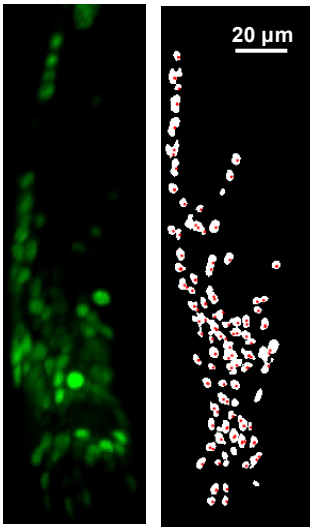

Figure S4: Microfluidic Array Device for Static Imaging

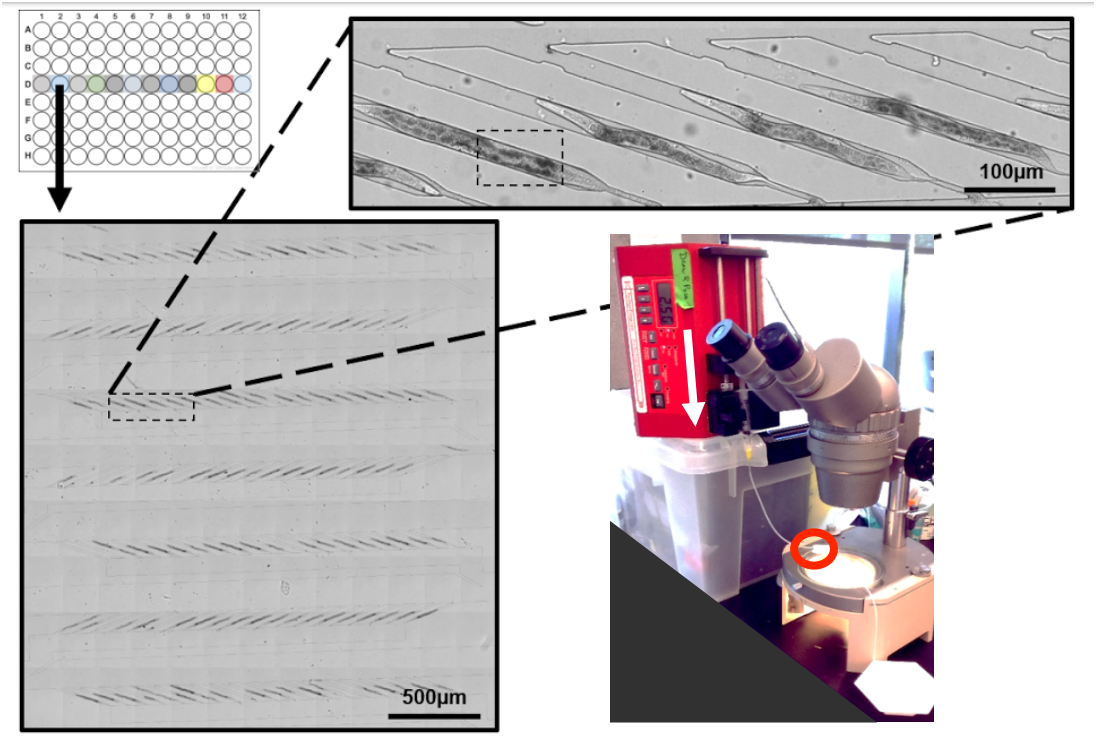

A microfluidic array device fabricated with 140 chambers is used to load the worms (Lee et al., 2014). To synchronize worms to the larval 4 (L4) stage, large plates of gravid adults are bleached. After ~ 48 hours, the intact eggs reach L4 stage and is ready for imaging. The worms are washed from the large plate, rinsed in 5mM tetramisole solution for 5 minutes for temporary immobilization, then withdrawn into the loading syringe. Using a pressurizer to control flow rate (2.5-5mL/hr), the microfluidic array device is first rinsed with M9 to degas, then switched to the loading syringe to load the worms. The microfluidic device is then brought to the microscopy lab for imaging. Array loading scheme is depicted. The red circle depicts the relative location of microfluidic device to the rest of the array loading set-up.

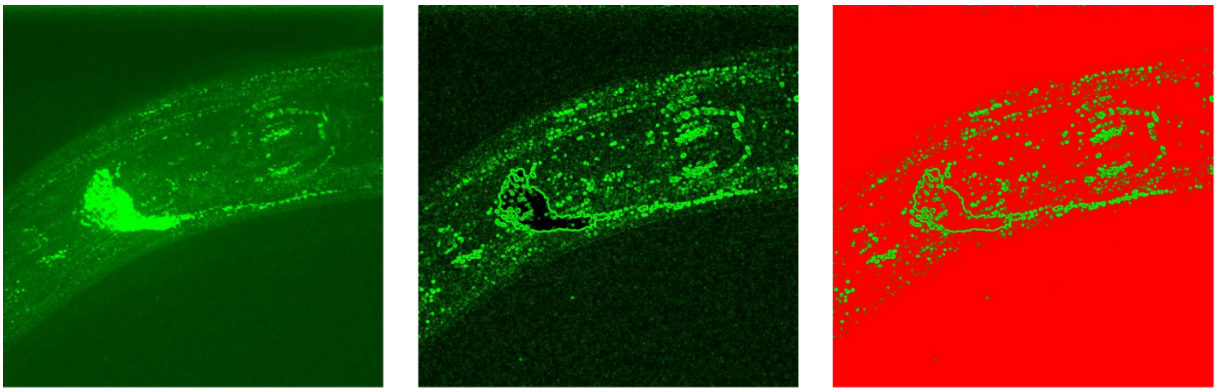

Raw Image → Detect Edges → Color Threshold (Intermodes)

Figure S5: Image Analysis Using ImageJ

A. Image Processing Pipeline to segment synapses into smaller particles. The biggest particle (active zone) overlays with the nerve ring.

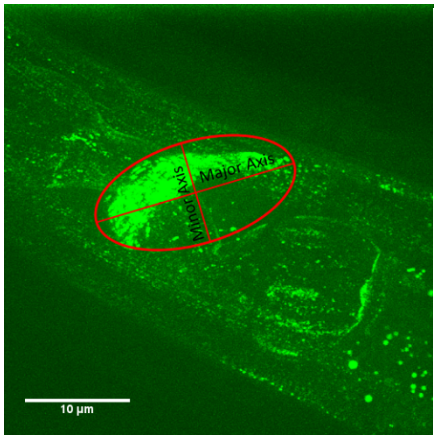

Representative image depicting features analyzed by Image J. The ellipse encircles the area of biggest active zone (AZ), where the nerve ring lies. Fit ellipse measures (major and minor axis) are highlighted with the red lines.

B. Fit Ellipse Measures on Synaptic Features